HYDRIDING OF TITANIUM

Second Annual Report (1997)

Contract No. N00014-96-1-0272

Submitted to
The Office of Naval Research
800 N. Quincy Street
Arlington, Virginia 22217

Submitted by
Clyde L. Briant, K. Sharvan Kumar, and Zhengfu Wang
Division of Engineering
Brown University
Providence, RI 02912

TABLE OF CONTENTS

ABSTRACT

This report presents a summary of the second year of work on ONR Contract N00014-96-1-0272, Hydriding of Titanium. The reason for undertaking this work is that the US Navy would like to use titanium in a number of critical applications, where it would come in contact with sea water at elevated temperatures. Although the general reputation of titanium is that it is corrosion resistant in these environments, there is the possibility that it could pick up sufficient hydrogen from this environment to form a hydride and thus lose its mechanical integrity. Therefore, we must evaluate all conditions that could lead to hydriding and determine the effects of hydrides on mechanical properties. During the second year of work, the goals have been the following: to determine the effect of solution activity and temperature, material composition and heat treatment on the electrochemical properties of titanium; to determine the effect of these same variables on the corrosion potential of titanium galvanically coupled with other metals; to determine the critical potential of hydride formation as a function of solution activity and temperature, applied strain, and surface conditions; to measure the rate of hydrogen diffusion in titanium; to propose a model to describe crack propagation in titanium in these environments. All of the above work has been completed and the results are contained in this document.

The results that we have obtained show that grade 2 titanium is generally resistant to hydrogen embrittlement. However, grade 3, with its higher interstitial content and lower hydrogen solubility is quite susceptible to hydrogen embrittlement. The mechanism by which this embrittlement occurs is one in which microcracks, which are centered on hydrides, form ahead of the main crack tip. With increased deformation these microcracks link up to the main crack and cause propagation. Since these hydrides do not form ahead of the main crack in grade 2 titanium but do form in grade 3 titanium, we are able to explain their different susceptibilities in this way. We also made measurements of the critical potential for hydride formation in grade 2 titanium. We found that the potential decreases from near -600 mV_{SCE} in solutions with a pH value of 1 to values of -1000 to -1200 mV_{SCE} in solutions with a pH value of 10. Temperature differences had a smaller effect on the critical potential. However, surface finish could have a significant effect on this potential. In addition to these effects, galvanic coupling and hydrogen diffusion in titanium were studied and discussed in this report.

1.0 INTRODUCTION

This report presents a summary of the second year of work on ONR Contract N00014-96-1-0272, Hydriding of Titanium. The overall goal of this project is to evaluate the performance of grade 2 titanium in sea water applications. The reason for undertaking this work is that the US Navy would like to use titanium in a number of critical applications, where it would come in contact with sea water at elevated temperatures. Examples would include condensers and heat exchangers in which sea water is used as a coolant. Although the general reputation of titanium is that it is quite corrosion resistant in these environments, there is the possibility that it could pick up sufficient hydrogen from this environment to form a hydride and thus lose its mechanical integrity. Therefore, we must evaluate all conditions that could lead to such hydriding and determine (a.) if the hydriding actually occurs and (b.) what affect the hydriding has on the properties of the material.

During the second year of work, the goals of the project have been the following.

- To determine the effect of solution activity, solution temperature, material composition and heat treatment on the electrochemical properties of titanium.
- To determine the effect of these same variables on the corrosion potential of titanium when it is galvanically coupled with other metals.
- To determine the critical potential of hydride formation as a function of solution activity, solution temperature, applied strain, and surface conditions.
- To measure the rate of hydrogen diffusion in titanium.
- To examine the effect of solution chemistry, material composition, and sample geometry on the mechanical properties of titanium when it is being dynamically charged with hydrogen.
- To propose a model to describe crack propagation in titanium in these environments.

All of the above work has been completed and the results are contained in this document.

2.0 EXPERIMENTAL PROCEDURE

Materials and Heat Treatment

The materials used in this study were commercially pure grade 2 and grade 3 titanium. Their chemical compositions are shown in Table I. These materials were supplied in the form of rolled sheets. The grade 2 material had a thickness of 1.12 mm and the grade 3 had a thickness of 0.62 mm. The as-received sheets were heat treated at 749°C for three minutes, followed by air cooling. Additional specimens of grade 2 titanium were divided into two lots and subjected to two different heat treatments. The first consisted of a 1000°C vacuum anneal for two hours followed by furnace cooling. The second consisted of 1000°C for 30 minutes in air, followed by water quenching. These were chosen because they substantially changed the grain morphology of the samples. The mechanical properties of materials used in this study are shown in Table II. Both the composition and the mechanical properties of the as-received material were supplied by the manufacturer.

Table I
Chemical Composition of Materials (wt.%)
(Balance of Composition is Titanium)

	Oxygen	Carbon	Nitrogen	Iron
Grade 2	0.14	0.02	0.008	0.08
Grade 3	0.21	0.01	0.009	0.16

Table II
Mechanical Properties of Materials

Material	Heat Treatment	Yield Strength (MPa)	Ultimate Tensile Strength (MPa)	Elongation (%)
Grade 2	As-received	344	506	28
Grade 2	Anneal/Furnace Cool	352	498	18
Grade 2	Anneal/Water Quench	524	524	2
Grade 3	As-received	489	603	24

Electrochemical Measurements

Electrochemical measurements, including the corrosion potential and the polarization curves, were performed at room temperature, 50°C, 70°C, and 90°C in aerated solutions of

6%NaCl and 3.5%NaCl with various pH values. The use of these solutions allowed us to study the effects of pH and NaCl concentrations on the electrochemistry of titanium. The solution of 3.5%NaCl with a pH of 8 closely resembles the salinity and pH of sea water.

The electrochemical measurements on titanium were performed on samples machined so that the area of exposure to the solution was 1 cm^2. When the titanium was galvanically coupled to another metal, a hole 6.5 mm in diameter, was machined into the center of the titanium tab, and a cylinder of the metal to which titanium was to be coupled was forced through the hole. The metals used to make these couples with titanium included HY80 steel, 316 stainless steel, five-nines aluminum, 6061 aluminum, and zinc. All specimens were mounted in epoxy resin to isolate electrical contact.

Each specimen surface was abraded with 600 grit silicon carbide paper immediately prior to testing to remove the surface oxide film. To make a measurement of the corrosion potential for both uncoupled and coupled titanium, the potential was controlled with a saturated calomel reference electrode (SCE). The specimen was held at -1400 mV_{SCE} for three minutes. Then, potential control was stopped and after two minutes the corrosion potential was recorded. In some cases we continued to monitor the corrosion potential as a function of time. In one set of experiments we also measured the effect of surface pre-treatment on the corrosion potential. These experiments were all performed using grade 2 titanium and the surface treatments included the as-received surface, finishing with 600 grit silicon carbide paper, samples pickled in 285 ml H_20 + 5 ml HNO_3 + 10 ml HF for 30 seconds, and an anodized sample. The anodized surface was prepared at the Titanium Finishing Company located in East Greenville, PA. The anodizing spec was AMS-2488B.

To measure the polarization curve we again held the sample at -1400 mV_{SCE} for three minutes and then left the potential uncontrolled for two minutes. A potential of -1800mV_{SCE} was then applied and the electrochemical potential was scanned at a rated of 10mV/min. to a final potential near -1200 mV_{SCE}, the exact value depending on the temperature of the solution.

Hydride Formation

A series of titanium samples was cathodically charged under different applied potentials in solutions of 6%NaCl with a pH value of 1 and 3.5%NaCl with various pH values. The tests were performed at room temperature, 50°C, 70°C, and 90°C for times of 24 to 168 hours. The purpose of these experiments was to obtain information on hydride formation. X-ray diffraction (XRD) was used to detect hydrides on the surface of individual samples after the charging procedure was complete. In all of the X-ray scans, we used Cu-Kα radiation (40kV, 35mA) and the scans were made between the angles of 34 and 45°. This range of angles

included peaks from both the δ- and γ-hydrides, the two most likely to occur under the conditions that we used.

In addition to the XRD measurements on the surface of the material, we also examined hydride growth into the sample. To make these measurements, we sectioned the sample perpendicular to the surface that was examined by XRD and polished it to a finish of 0.5μm. The hydrides were revealed by etching the sample in a solution of 285 ml H_20 + 5 ml HNO_3 + 10 ml HF. The hydrides could be observed both optically and in the scanning electron microscope.

Hydrogen Diffusion

The materials used in this study were titanium foils with a thickness of 50μm. Two different materials were used; one had a purity of 99.96% and the other had a purity of 99.99%. We will refer to them as the low purity (LP) and high purity (HP) materials. One set of LP samples was used in the as-received condition and the other foils were pickled in the solution described previously. To make the diffusion measurements, we first coated one side of the sample with a thin layer of pure titanium and then on top of this layer we deposited a 1μm layer of palladium. The palladium was required to prevent oxidation of the titanium during the diffusion measurements; such coatings are frequently used in these types of measurements and have been shown not to affect the diffusion of hydrogen [1]. The initial coating of titanium was required to have good electrical contact between the palladium and the titanium. Both depositions were performed using an electron beam evaporator with a vacuum below $1x10^{-6}$ torr.

The measurement of hydrogen diffusion was conducted in an electrolytic permeability cell [2,3] as shown in Figure 1. The cell consisted of two identical compartments clamped together at the foil specimen. At this connection O-rings were used to ensure leak-free connections. Each compartment contained a Pt wire counter electrode, a reference electrode, and a Luggin capillary probe. The potential of each side of the specimen was controlled by separate potentiostats. Temperature was maintained constant by immersing the cell in oil for which the temperature was controlled to 70°C.

To begin the experiments, a 0.1N NaOH solution was introduced into both compartments of the cell. Nitrogen, which had been purified by passing it over hot copper turnings, was bubbled through both solutions for at least six hours to remove oxygen. The side of the foil that was coated with palladium was anodically polarized at a potential of 200 mV_{SCE} for 12 hours to obtain a stable anodic current before testing. This anodic current was very small because most oxygen had been removed from the solution and the titanium was

covered by the palladium. This background current was subtracted from the measured current during testing. The other side of the foil was cathodically polarized at a potential of either -1500 mV_{SCE} or -1800 mV_{SCE} to provide a constant hydrogen source. The hydrogen generated on this side of the sample would diffuse through the material to the anodic side and be ionized and recorded in the anodic current.

Figure 2 shows a typical hydrogen permeation curve. The transient analysis enables the diffusion coefficient D to be evaluated from the relationship

$$t_1 = L^2/6D \qquad (1)$$

where L is the thickness of the samples and t_1 is the time at which the permeation flux, J, attains a value of 0.63 of the steady-state permeation[4].

Mechanical Tests

The mechanical tests were performed with the samples in solutions of 6%NaCl at a pH value of 1 and in 3.5%NaCl at a pH value of 7. The temperature of the solution was 70°C. Sheet tensile samples were cut that had a width of 11.43 mm in the gage section. Most samples were cut from the as-received sheet so that the length of the sample was perpendicular to the rolling direction and contained a notch that was 2.54 mm deep and subtended an angle of 60°. To examine the effect of notch angle and material orientation, we tested some samples that were cut with their length parallel to the rolling direction or samples that had a notch angle of 20°. The thickness of the samples was that of the original sheet from which they were cut. The center part of the specimen was polished with 600 grit silicon carbide paper and degreased with acetone. The remainder of the gage section was coated with silicone to limit the area of exposure during the test.

Figure 3 shows the set-up for the mechanical tests, which included an electrolytic cell placed on an Instron testing machine. The reference electrode was placed in a small beaker containing the test solution at room temperature and was connected to the actual test solution through a Luggin probe. The electrochemical potential of the exposed area of the sample was controlled to the desired potential in this way. Initially, the sample was held at -1400 mV_{SCE} for three minutes in the 70°C solution, the potential was then set to the specified value, and the samples was strained slowly to failure at a fixed crosshead speed. The susceptibility of a material to hydrogen embrittlement was determined from the ratio of the elongation-to-failure in solution to the elongation-to-failure in oil at the same temperature. The parameter will be referred to as the elongation ratio in the rest of this report.

3.0 RESULTS AND DISCUSSION

Electrochemical Measurements

Figure 5 shows the corrosion potentials for grade 2 and grade 3 titanium in 6%NaCl solution (ph=1) and in 3.5%NaCl (pH=8) plotted as a function of temperature. For grades 2 and 3 in the as-received condition, the corrosion potential increased with increasing temperature of the solution. Similarly, the corrosion potential increased for each grade with increasing solution acidity. For a given pH, however, grade 3 exhibited a higher corrosion potential at all temperatures. As the primary difference between the two grades is the oxygen and iron content, this trend might indicate that the corrosion potential of titanium increases with increasing levels of these impurities.

The measured value of the corrosion potential depended on testing time. The values shown in Figure 5 were obtained after three minutes of cathodic polarization at -1400mV_{SCE} and then two minutes at the free corrosion potential. Figure 6 shows the variation of the corrosion potential with testing time for grade 2 titanium in 3.5%NaCl solution and synthetic sea water at different temperatures. On this curve the zero time point corresponds to the corrosion potential after two minutes reported above. At each temperature, the corrosion potential generally increased with increasing time and reached a relatively stable value after approximately one hour. This increase in the corrosion potential was probably caused by the formation of an oxide film on the surface of the sample. We also found that the value of the corrosion potential after longer times were more scattered and that the effects of pH and temperature were less evident. This difference can again be attributed to the formation of the oxide film.

Titanium in salt water has a very low rate of film dissolution, and the film has been reported to be stable even at the boiling point of some solutions[6-8]. There is some disagreement on the effect of pH on film dissolution. Shreir[6] reported that complete breakdown does not occur even at very low values of pH, although Covington[9] stated that the oxide film on titanium is totally dissolved at pH values below 3. Regardless of the degree of oxide film disintegration, it is reasonable to assume that low pH values tend to promote the dissolution and thus could promote corrosion of titanium. Therefore, it would appear that the appropriate way in which to interpret our results is the following. The increase in corrosion potential with temperature, for a given pH value, probably results from the increase in the cathodic reaction rate and not because of an increase in the anoidc reaction that could come from film breakdown. This interpretation is consistent with the results of the polarization curves. The increase in the corrosion potential with pH can be attributed to both the increase in

corrosion of titanium and an increase in the exchange current density for the hydrogen reduction reaction. These points are shown shcematically in Figure 15.

Figures 7-12 represent the polarization curves for grade 2 titanium in 6%NaCl (pH=1) and 3.5%NaCl (pH=1, 4, 7, 8, and 10). On each plot curves are given for different temperatures. Figures 13 and 14 show the polarization curves for grade 3 titanium in 6%NaCl (pH=1) and 3.5%NaCl (pH=8), again measured at different solution temperatures. In all solutions, the cathodic reaction rate tended to increase with temperature. Moreover, a comparison of the cathodic reaction rates for a given grade showed that this process was enhanced by increased acidity of the solution. There was not a significant difference between the curves for grade 2 and grade 3 titanium when tested under the same condition.

In all cases the corrosion potentials determined by the polarization curves were higher than those obtained from the direct corrosion potential measurements. Again we feel that this difference arises from the different types of surface preparation used for the two different test methods and the rate at which the oxide forms on the surface. This point is discussed in reference 5.

The polarization curves help determine the types of cathodic reactions that take place at different potential regimes. The main cathodic reactions that can occur in aqueous solutions are the reduction of dissolved oxygen, the reduction of hydrogen ions, or the direct reduction of water. The latter two can cause hydrogen evolution. At any given potential-pH combination one of these reactions will dominate and determine the current density measured on a polarization curve. Figure 16 schematically shows a polarization curve with the different cathodic reactions described above. At a potential above point 1, the reduction of dissolved oxygen is the dominant cathodic reaction. At the potential between points 1 and 2 hydrogen reduction will be the dominant reaction. Below point 2 the dominant cathodic reaction will be direct reduction of water. Whether or not one observes these reactions will depend on the pH of the solution. At very low pH values, the reduction of dissolved oxygen will not be observed. In neutral or alkaline solutions, the hydrogen reduction reaction will not be observed and direct reduction of water follows directly from reduction of dissolved oxygen. Tables III and IV show the potential values at which points 1 and 2 occur for grade 2 and grade 3 titanium, respectively. These results show that as the pH decreases, the potential at which hydrogen could be generated decreases.

Effect of Heat Treatment

The corrosion potentials for heat treated grade 2 samples in both the furnace-cooled and water quenched conditions in 3.5%NaCl (pH=8) are shown in Figure 17. The corrosion potential of titanium subjected to these heat treatments exhibited essentially no temperature

dependence, as the variation of corrosion potential with temperature lay within the normal scatter range of the data. Additionally, the corrosion potentials of both heat-treated specimens were significantly higher than those of the as-received titanium at room temperature and 50°C but lower at 70 and 90°C.

Figure 18 shows the polarization curve for heat treated grade 2 samples in both the furnace-cooled and water quenched conditions in the same solution at different temperatures. The corrosion potential and cathodic reaction rate of annealed and furnace cooled grade 2 titanium were unaffected by solution temperature. The anodic reaction rate of this heat-treated sample showed no clear trend with increasing temperature. The polarization curve for the annealed and quenched grade 2 titanium exhibited an essentially constant corrosion potential throughout the temperature range, but displayed a slight increase in both cathodic and anodic reaction rates with temperature. Thus, the microstructural variation produced by these heat treatments appeared to fix the corrosion potential but not necessarily eliminate the effect of temperature on the cathodic reaction rate.

Figure 19 shows the microstructures of grade 2 titanium in the as-received and the two heat treated conditions. The annealed specimens exhibited considerable grain growth. The as-received sample had an average grain size of 26μm whereas the quenched sample had a grain size of 48μm and the furnace cooled sample had a grain size of 68μm. More interestingly, the annealed specimens exhibited a definite change in the morphology of the microstructure. In the as-received condition, the grade 2 material had an equiaxed grain structure, whereas the heat-treated microstructures contained grains that were comprised of aligned needles or platelets. These features were coarser in the furnace-cooled specimen, but both samples had a similar appearance.

Long Time Data and Effect of Surface Condition

Figure 6 indicated that the corrosion potential reached a relatively stable value after the sample was exposed to a solution for about one hour. However, this value could change over the long service times that are required for engineering applications. Figure 20 shows the corrosion potential in 3.5%NaCl (pH=7) at room temperature for up to four weeks. The corrosion potential for the sample with the abraded surface (the same condition used in all experiments described above) continued to increase through the first week of exposure in solution and then gradually reached a stable value.

Figure 20 also shows the effect of surface condition on the corrosion potential as a function of time. The corrosion potential for the pickled, anodized, and as-received surfaces changed slightly during the exposure time. The sample with the pickled surface had a higher corrosion potential compared to the other two samples. However, the corrosion potentials for

Table III

Potential at point 1 and 2 for grade 2 titanium in 6%NaCl and 3.5%NaCl solutions at different temperature

Point	Temperature	Potential mV_{SCE}					
		6%NaCl	3.5%NaCl				
	°C	pH=1	pH=1	pH=4	pH=7	pH=8	pH=10
1	23	/	-600	/	/	/	/
	50	-700	-600	/	/	/	/
	70	-700	-600	/	/	/	/
	90	-400	-600	/	/	/	/
2	23	-1500	/	/	-1200	-1400	-1200
	50	-1600	/	-1200	-1200	-1200	-1100
	70	-1600	/	-1200	-1200	-1200	-1100
	90	-1200	/	-1200	-100	-1100	-1100

Table IV

Potential at point 1 and 2 for grade 3 titanium in 6%NaCl and 3.5%NaCl solutions at different temperature

Point	Solution	Potential mV_{SCE}			
		23 °C	50 °C	70 °C	90 °C
1	6%NaCl (pH=1)	-600	-600	-600	
	3.5%NaCl (pH=8)	/	/	/	/
2	6%NaCl (pH=1)	/	/	/	
	3.5%NaCl (pH=8)	-1400	-1200	-1100	-1000

all of these samples was lower than the final potential of the sample with the abraded surface. In all cases we attribute the change in the corrosion potential with time to changes in the oxide on the surface of the metal when it is exposed to the NaCl solutions. Thus, the fact that the abraded sample changed more as a function of time and also exhibited the highest corrosion potential suggests that the initial state of this surface was significantly different from the other samples and that the oxide that evolved with time was different either in composition or character from that present on the other surfaces.

Titanium Coupled With Other Metals

The corrosion potentials of grade 2 titanium galvanically coupled with naval brass, HY80 steel, 316 stainless steel, five-nines aluminum, 6061 aluminum, and zinc in 6%NaCl (pH=1) and 3.5%NaCl (pH=8) are plotted as a function of temperature in Figures 21 and 22, respectively. In the 6%NaCl solution the naval brass couple exhibited a corrosion potential greater than that of uncoupled grade 2 titanium; naval brass caused titanium to become an anode. At room temperature, HY80 steel and 316 stainless steel couples exhibited corrosion potentials greater than that of uncoupled titanium but exhibited lower corrosion potentials at higher temperatures. In these couples titanium was the anode at room temperature and the cathode when the temperature was increased. However, the individual corrosion potentials for the two dissimilar metals were close and the driving force for this galvanic corrosion was small. Five-nines aluminum and 6061 aluminum had nearly the same electrochemical behavior in this solution and caused cathodic polarization of the titanium. The corrosion potentials of these couples were not strong functions of temperature, as both types exhibited an essentially constant potential of -800mV_{SCE} over the temperature range that we investigated. Zinc couples caused the most extreme cathodic polarization of the titanium. The couples exhibited an essentially constant corrosion potential near -1075 mV_{SCE} over the temperature range that we investigated.

The behavior of these couples in 3.5%NaCl (pH=8) followed the trends described above with the following exceptions. First, the 316 stainless steel assumed the role of the anode in the pair over the entire temperature range. Secondly, the five-nines aluminum couple exhibited a much stronger dependence on temperature, as its corrosion potential dropped 200mV_{SCE} over a range of 70°C.

Corrosion potentials for grade 3 titanium coupled with the same metals in 6%NaCl (pH=1) and 3.5%NaCl (pH=8) are plotted as a function of temperature in Figures 23 and 24. In both 6%NaCl and 3.5%NaCl solutions, the temperature dependence of the corrosion potentials of the couples were similar to those of the grade 2 titanium couples. However, as shown in Figure 5, uncoupled grade 3 titanium exhibited a higher corrosion potential than

grade 2 in both solutions. Again, the five-nines aluminum couple exhibited a much stronger temperature dependence in 3.5%NaCl than in the 6%NaCl solution. Moreover, grade 3 titanium coupled with naval brass, 316 stainless steel, or HY80 steel in both 6%NaCl and 3.5%NaCl solutions exhibited a corrosion potential below that of uncoupled titanium at elevated temperatures.

From the above results we found that solution composition and pH value did not change the corrosion potential significantly. However, the change from grade 2 to grade 3 caused titanium to become a cathode at all temperatures when coupled with naval brass, HY80 steel and 316 stainless steel. When the titanium is a cathode, it is possible that hydrogen will evolve on its surface, possibly leading to hydride formation. The occurrence of these hydrides will be discussed in subsequent sections of this paper.

Figure 25 shows the corrosion potentials of grade 2 titanium galvanically coupled with HY80 steel, five-nines aluminum, and zinc in 3.5%NaCl (pH=7) at room temperature plotted as a function of time for tests that lasted for four weeks. The corrosion potentials for HY80 steel and zinc couples kept constant for the entire period of time. They remained at approximately -610 mV_{SCE} and -990 mV_{SCE}, respectively. The corrosion potential for the five nines aluminum couple decreased by approximately 100 mV_{SCE} after two weeks exposure in solution. The final corrosion potential was approximately -800 mV_{SCE}. These values are all similar to those shown in Figure 22.

During the long time measurments, we did not observed visible hydrogen evolution from the sample surface. However, we did observe corrosion products coming from the disc, especially the one made from zinc. After four weeks exposure the discs were removed and titanium samples were examined by X-ray diffraction. Figure 26 shows the pattern obtained from the titanium coupled with HY80 steel, five-nines aluminum, and zinc after being exposed in 3.5%NaCl (pH=8) solution at room temperature for four weeks. This pattern showed a significant hydride (γ) peak from titanium coupled with zinc, a small hydride (γ) from titanium coupled with five-nines aluminum, and no hydride peak from titanium coupled with HY80 steel.

Critical Potential for Hydride Formation

If one examines the literature on hydrogen embrittlement of titanium, it appears that hydride precipitation is required to obtain significant degradation of mechanical properties. However, hydrogen in solid solution also has been reported to affect the mechanical properties [13], so it is important to obtain information on the potentials at which hydrogen absorption is observed and those where significant hydride formation occurs. The results in the literature are

somewhat contradictory. First let us consider hydrogen absorption. Covington[9] indicated that hydrogen absorption occurred in natural sea water only when titanium had a potential lower than approximately -700 mV_{SCE}. Fukuzuka[10] reported a limiting potential for hydrogen absorption of -750 mV_{SCE} in aerated sea water at 25°C and -650 mV_{SCE} in deaerated sea water at 100°C. Similar results were obtained by Satoh[11] who reported that the limiting potential for hydrogen absorption was -750 mV_{SCE} in natural sea water. Experiments by Nosetani[12] in artificial sea water at ambient temperature showed that no hydrogen absorption was detected after three months at a potential of -600 mV_{SCE}, below 20 ppm at -800mV_{SCE} and 100-200 ppm at -1000 to -1200 mV_{SCE}.

In the case of hydride formation, less infomration is available. Experiments by Schutz and Grauman[18] indicated that significant hydriding of titanium in neutral sea water only occurred at potentials lower than -1200mV_{SCE}. A limit of -1000 mV_{SCE} was suggested for avoiding significant hydriding of titanium in sea water below 45°C. However, detailed research concerning the critical potential for hydride formation under various conditions has not been studied in detail. For this reason we have completed an extensive study of the critical potential required to cause hydride formation under specific conditions.

For these studies titanium samples were charged in sodium chloride solutions for 24 hours at different temperatures under controlled potentials. After being charged, the samples were examined by X-ray diffraction (XRD) to determine if hydrides could be found. Figure 27 shows a typical set of data. This particular example is for grade 2 titanium after it was cathodically charged in a 3.5%NaCl (pH=1) solution under potential control at 90°C. Hydrides were first detected at -600 mV_{SCE}, and at all potentials lower than this value, they were observed. Above this value, the XRD patterns were similar and showed no evidence of hydride formation. Thus we would define the critical potential for grade 2 titanium in this solution at this temperature as -600 mV_{SCE}.

Figure 28 shows the variation of the critical potential for hydride formation for grade 2 titanium in 3.5%NaCl plotted as a function of temperature. The different lines are for different values of pH. In the solution with a pH value of 1, the γ-hydride, TiH, was first detected by XRD at -600 mV_{SCE} at all temperatures. The δ-hydride, TiH_2, was first detected at -700 mV_{SCE} at room temperature, but was also detected at -600 mV_{SCE} at 50, 70, and 90°C. In solutions with pH values above 1, only the γ-hydride was detected. In these solutions the critical potential remained constant at 50°C and room temperature but increased with increasing temperatures above 50°C. The results in Figure 28 also show that in general pH was a much more important variable than temperature. In particular, there was a significant decrease in the critical potential between pH values of 1 and 4.

The absorption of hydrogen and the subsequent hydride formation can be affected by the surface condition. Figure 29 shows the critical potential for hydride formation for grade 2 titanium in 3.5%NaCl plotted as a function of pH. All tests were performed with the solution at 70°C. For all surface conditions, the critical potential for hydride formation decreased with an increase of the pH value. However, this decrease depended on the surface treatment. The abraded surface had the highest potential, followed by the anodized surface, the pickled surface, and the as-received surface in that order. The difference between the highest and lowest critical potentials increased with increasing pH. The difference was 100 mV in the solution with a pH value of 1, but became as high as 500 mV in the solution with a pH value of 10. This last point emphasizes the important effect of pH on hydride formation.

We finally make a comparison between the critical potential for grade 2 and grade 3 titanium. The critical potential for grade 2 titanium in 6%NaCl (pH=1) at 70°C was -600 mV_{SCE}. The concentration of NaCl in solution did not have a significant effect on this value as reported in our 1996 annual report[5]. Figure 30 shows the critical potential for grade 3 titanium in 6%NaCl (pH=1) at 70°C. The value for this potential was -700 mV_{SCE}. The difference in the material may have a slight change on the critical potential, but it does not appear to be a significant effect.

Kinetics of Hydriding

Grade 2 titanium samples were cathodically charged at a potential of -1400 mV_{SCE} in 3.5%NaCl solution with pH values of 1 and 7 at 70°C for up to seven days. The hydride phases were examined by XRD tests and the thickness of the hydride film on the surface was measured by SEM. Figures 31 and 32 show XRD patterns obtained from the solution with pH values of 1 and 7, respectively. The δ-hydride formed in the pH=1 solution and γ-hydride was formed in the pH=7 solution. In either case the stoichiometry of the hydride was TiH_x. Millenbach and Givon[19] indicated that the value of X increased with the cathodic charging current density. Phillips[20] and Wu[21] also indicated that X increased with increasing current density. At the applied potential of -1400 mV_{SCE}, the charging current density in the pH=1 solution was much larger than that in the pH=7 solution. This result is consistent with the δ-hydride being formed in the lower pH solution, since it has a higher hydrogen content that the γ-hydride.

However, pH may not be the single controlling factor. Otsuka[22] reported that the composition of surface layers of hydride during the corrosion of titanium in various aqueous solutions depended on the corrosive environment and covered almost the entire range from TiH to TiH_2. Tomashov[23] has shown that at a charging current density of 5 mA/cm^2, the

maximum hydrogen content of the hydride film occurred and that a further increase in the charging current density had little effect on hydriding. The upper limit of stoichiometry corresponded to TiH_2.

Figures 33 and 34 show the microstructure of the hydrides for the specimens cathodically charged in the pH=1 and pH=7 solutions for seven days. In the pH=1 solution the hydrides formed on the titanium surface and penetrated into the titanium matrix. Presumably as a result of the volume increase in the hydride relative to that of the matrix, the hydrides formed in this solution cracked extensively. In the pH=7 solution, the hydrides were observed to penetrate into the titanium matrix, but no obvious hydride film could be observed on top of the surface and it was not possible to measure a thickness. The hydrides formed in both solutions had a lath-like appearance. All hydrides were formed near the surface, and none were found beneath this surface layer in the bulk.

Figure 35 shows the relationship between the thickness of the hydride in the pH=1 solution and hydrogen charging time. The growth rate appeared to be parabolic. This result suggests that once the hydride film formed on the surface, it resisted further hydrogen penetration. Phillips' results[24] suggest that the growth rate is parabolic with time.

Hydrogen Diffusion

Hydrogen diffusion in metals is generally studied by measuring the rate of transport of hydrogen past a solid-gas interface at a relatively high temperature[25,26]. At low temperatures, however, the measured rate may be surface-controlled and the calculated diffusion coefficients will be in error. The measurements of hydrogen diffusion at low temperatures (below 100°C) can be carried out by an electrochemical method. This method was first developed by Devanathan and Stachurski[2,3] who created a cell in which hydrogen evolved on the cathodic side of a bi-electrode membrane and oxidized the permeating hydrogen anodically on the other. Brauer et al.[27] were the first to use this method to study hydrogen diffusion in titanium. The diffusion coefficient that they measured, $2x10^{-7}$ cm^2/s, was about five orders of magnitude higher than estimates from previously published studies on diffusion in α-titanium[20,28]. They attributed the difference to the possible effects of hydride formation, the presence of oxide surface layers, and impurities in previous studies. Phillips et al.[20] determined the hydrogen diffusion coefficient in titanium to vary between $4x10^{-12}$ to $5x10^{-10}$ cm^2/s in the temperature range of 25 to 100°C. These values were obtained by measurements of the thickness of the growing hydride layer as a function of time. Recent results by Abdul-Hamid and Latanision[29] using the electrochemical method indicated that the diffusion coefficient for hydrogen at 30°C was $2.6x10^{-10}$ cm^2/s. They proposed that hydrogen

diffused by an interstitial mechanism but that diffusion along grain boundaries would be significantly faster.

We now consider the results that we obtained by using the electrochemical method to measure the hydrogen diffusion rate at 70°C. Figure 36 shows the permeation current plotted as a function of time. This plot is for the low purity material with the cathodic side of the sample held at an electrochemical potential of -1500 mV_{SCE}. The permeation current increased with increasing time and reached a steady state after 50 hours. The hydrogen diffusion coefficient can be calculated from this curve using equation 1 and found to be $9.9x10^{-11}cm^2/s$. This value was lower than that obtained by others using this electrochemical method[27,29] but is consistent with past work that employed other techniques. The sample surface was examined by XRD after the test and no evidence of hydride precipitation was observed. Therefore, the lower value could not be attributed to the presence of this phase.

Figure 37 shows the variation of permeation current from a pickled low purity sample charged at 70°C at a potential of -1800 $_{mVSCE}$. The calculated hydrogen diffusion coefficient was $7.6x10^{-11}cm^2/s$. This value was smaller than that obtained from the data plotted in Figure 36. The sample surface was examined by XRD after the test and a small γ-hydride peak was observed, Figure 38. This hydride could have inhibited hydrogen diffusion. Figure 39 shows that no hydrogen permeation current could be detected when the as-received low purity sample was used. The thick oxide on this sample inhibited diffusion into the sample.

Figure 40 shows the variation of the permeation current from the pickled high purity sample that was charged at 70°C and at a potential of -1500mV_{SCE}. The calculated hydrogen diffusion coefficient was $3.6x10^{-11}cm^2/s$. This lower value suggests that hydrogen diffusion decreased with increasing purity of the sample.

Mechanical Tests

We now consider the results of the mechanical tests. Figure 41 shows the elongation ratio plotted as a function of applied potential. Data are shown for both grade 2 and grade 3 material. (Both the values of elongation in the solution and in oil were obtained at the same crosshead speed, since we found that the elongation to failure depended strongly on this variable. For example, the elongation to failure in oil increased by 7% when the crosshead speed decreased from $7x10^{-2}$ to $7x10^{-4}$ mm/min.) The main conclusion to be drawn from this figure is that the elongation to failure decreased for grade 3 titanium as the potential became more cathodic whereas for grade 2 there was little effect. The difference was especially noticeable below -800 mV_{SCE}. At these low potential values, significant quantities of hydrogen should be generated and both materials were capable of forming hydrides. However, the effect

of hydrogen on mechanical properties was much greater for grade 3 than for grade 2. Several additional points should be noted. The data for grade 2 titanium were obtained at two different crosshead speeds. The data obtained at $7x10^{-4}$ mm/min are directly comparable to the data obtained for grade 3. Also, it should be noted that the actual time required to perform the test was much longer for the grade 2 material, even at the higher crosshead speed, because of its lack of susceptibility to hydrogen cracking.

We also investigated the effect of crosshead speed on the susceptibility to hydrogen embrittlement. Usually, hydrogen embrittlement increases with decreasing crosshead speed because the hydrogen has more time to diffuse to the crack tip. Figure 42 shows the elongation ratio plotted as a function of crosshead speed at an applied potential of -1400 mV_{SCE}. Very little change was observed for grade 2 as the crosshead speed was decreased over several orders of magnitude. By comparison, the elongation ratio for grade 3 titanium decreased by approximately 60% over the same range of crosshead speeds. Thus, decreasing both the applied potential and crosshead speed has a significant effect on the hydrogen embrittlement of grade 3 titanium but not on that of grade 2.

The thickness of the hydride layer on the surface of the mechanical test samples was measured by SEM after the sampled failed. The thickness varied with applied potential and crosshead speed. Figure 43 shows the variation of the thickness of the hydride layer on the sample surface for grade 3 titanium plotted as a function of applied potential. The hydride film was initially detected at a potential of -700 mV_{SCE}, and its thickness increased as the applied potential decreased. Note that the film thickness at low potentials was significantly higher, even though the time of exposure was shorter. The average hydride layer growth rate could be determined from the thickness of the hydride layer and the total testing time, if one assumes that nucleation of the hydride phase required an insignificant amount of the total time. This trend is shown in Figure 43, with the average hydride layer growth rate increasing with decreasing applied potential. Figure 44 shows the variation of the thickness of the hydride layer on the sample surface for grade 2 and grade 3 titanium plotted as a function of crosshead speed at a controlled potential of -1400mV_{SCE}. The thickness on both metal surfaces increased with decreasing crosshead speed. A low crosshead speed allowed much greater time for hydride formation and resulted in a very thick hydride layer on the sample surface. However, it was interesting to note that, although the thickness of the hydride layer on the sample surface for grade 2 increased with decreasing crosshead speed, the elongation obtained in solution for this metal remained essentially constant, as shown in Figure 42. This result implies that the hydride film on the sample surface had little effect on the mechanical properties of the notched tensile samples that were used. Figure 45 shows the average hydride layer growth rate for the two materials plotted as a function of the crosshead speed at an applied potential of

-1400 mV_{SCE}. Although the thickness of the hydride layer increased with decreasing crosshead speed, the average hydride layer growth rate decreased with decreasing crosshead speed. This result indicated that the ease of hydride phase formation decreased with increasing time. This result is consistent with the results above. It is concluded that once the hydride films forms, this layer resists further hydrogen penetration. It should be noted that the difference observed in the hydride growth rate for grades 2 and 3 at high crosshead speeds is primarily an effect of the longer test time required for grade 2; also, at these high crosshead speeds, the hydride layer was very thin and there could be more scatter in our measured value.

Hydrides formed on the fracture surfaces of tests pieces, and away from the crack tip the thickness could be quite significant. Figure 46 shows the hydride layer on the crack wall for grade 3 titanium after it was tested at a potential of -1400 mV_{SCE} and a crosshead speed of $7x10^{-4}$ mm/min. Such a layer was not observed when the tests were run at a potential of -700 mV_{SCE}.

The fracture surfaces of all samples of grades 2 and 3 titanium tested at potentials above -700 mV_{SCE} were ductile and similar to those for samples tested in oil, regardless of the crosshead speed. Figure 47 shows the typical appearance of this kind of fracture surface; one can observe the presence of many slip bands. More negative applied potentials resulted in an increase in the hydrogen embrittlement susceptibility, especially for grade 3, but also resulted in a thicker hydride layer on the fracture surface. Thus, some features could not be clearly observed on the fracture surface when it was examined after the test was completed. Figure 48 shows the typical appearance of the fracture surface of grade 2 at a potential of -1200 mV_{SCE} and of grade 3 titanium at a potential of -1400 mV_{SCE}, both tested at a crosshead speed of $7x10^{-4}$ mm/min. The surface exhibited many secondary cracks and voids In addition, the slip bands could be observed on the fracture surface, which indicated that plastic slip still occurred at the crack tip at an applied potential as low as -1400 mV_{SCE}. Although these cracks appeared to be brittle, the elongation of grade 2 titanium decreased only slightly relative to that measured in oil.

Mechanical tests were also performed on grade 2 titanium to assess the effect of solution composition, pH value, notch radius, and texture. We first consider the effect of solution composition. Figure 49 shows the elongation ratio plotted as a function of crosshead speed for grade 2 titanium in 3.5%NaCl at a pH value of 8. The temperature of the solution was 70°C and the electrochemical potential was -1400 mV_{SCE}. The ratio decreased with decreasing crosshead speed. However, all values for the ratio were above 90%. In all cases the fracture was ductile, although a few secondary cracks could be observed for the sample tested at a crosshead speed of $7x10^{-4}$ mm/min. These results were very similar to those for grade 2 titanium tested in 6%NaCl solution with a pH value of 1, as shown in Figure 41. We

also found that, in general, the thickness of the hydride film on the sample surface increased with decreasing crosshead speed. However, as we will show below, in these notched specimens the hydrogen embrittlement susceptibility was not dependent on the thickness of the hydride film on the unstrained surface, but was dependent on the thickness of the hydride film at the crack tip and the presence of hydrides in the area ahead of the crack tip. In these samples no visible hydrides were found at the crack tip or in the area ahead of it.

Figure 50 shows the effect of notch angle and sample orientation on the elongation ratio for grade 2 titanium in 6%NaCl (pH=1) at 70°C and -1400 mV_{SCE}. The crosshead speed was $7x10^{-4}$ mm/min. The elongation ratio is shown in each case. The values obtained were all above 90%, which indicates that neither of these variables has a strong effect on hydrogen embrittlement susceptibility.

4.0 MECHANISM OF HYDROGEN EMBRITTLEMENT

In hydride forming systems, hydrogen embrittlement is reported to occur by the formation of the hydride at points of stress concentration, followed by the cracking of this hydride phase. This fracture usually appears to be cleavage-like cracking that occurs either through the hydride phase or along the hydride-matrix interface[30,31,39-42]. The hydride phase is reportedly brittle and has different elastic properties from the parent lattice. Hydride films on the surfaces of samples will crack when the specimen is tested in tension. In both grades 2 and 3 titanium we found hydrides on the surfaces of the samples. Although the elongation ratio for grade 3 titanium decreased relative to the value measured in oil when tested at sufficiently cathodic potentials, this parameter remained essentially unchanged for grade 2 titanium, so simply the formation of the hydride is not sufficient to cause embrittlement. We now seek to find reasons for this difference.

In the notched samples that we tested, the hydrogen embrittlement was not dependent on the thickness of the hydride film on the unstrained surface, but one could hypothesize that a correlation could be established between susceptibility to hydrogen embrittlement and hydride thickness at the crack tip. However, if the hydride is to play a significant role in the crack propagation, it must form quickly on the newly exposed surface. The micrographs in Figure 51 show the cross-section of the specimen along the loading direction after failure for grade 3 titanium tested at a potential of -1400 mV_{SCE} and using a cross head speed of $3.5x10^{-4}$ mm/min. The crack shown here was not the main crack but rather one that had formed along the gauge length of the specimen; the propagation rate of this crack was much smaller than the propagation rate of the main crack. Figure 51 clearly shows that there is no hydride phase on the surface at the crack tip. Since we assume that this crack is growing more slowly than the main crack, we must conclude that extensive surface hydride formation at the crack tip is not playing a significant role in the process.

We now consider the hydride distribution as a possible cause of the different hydrogen embrittlement response of the two materials. Our annual report for 1996[5] showed than in grade 2 titanium, hydrides formed on the surface of the sample and penetrated into the titanium matrix. The thickness of the hydride layer varied with testing conditions such as solution temperature, pH value, solution chemistry, applied potential or current density, and hydrogen charging time. The hydrides in grade 2 titanium were all associated with this surface layer. We did not observe individual or groups of hydrides in the interior of the sample separated from this surface layer. The hydride layer on the surface of grade 3 titanium was identical to those for grade 2 titanium; however, hydrides could also be observed in the interior of grade 3

titanium that were separate from the surface layer. Figure 52 shows the microstructure of the hydrides from a grade 3 titanium specimen which was cathodically charged at a potential of -1400 mV_{SCE} for five days. Individual hydride laths could be observed in the interior well beyond the surface layer. Since these interior hydrides are not present in grade 2 titanium, this difference could explain the difference in susceptibility. Since the main difference between these two materials is chemical composition, we now propose to relate the difference in hydride formation and distribution to this difference in composition.

In general, embrittlement-resistant alloys appear to display a combination of high hydrogen solubility and low hydrogen diffusivitiy. The former avoids hydride precipitation and the latter slows down the rate at which the critical concentration for hydride formation in the matrix can be reached. For commercially pure titanium, the largest impurity constituent is oxygen, which is an interstitial element. The grade 3 material that we used contained 50% more oxygen than the heat of grade 2. Carbon and nitrogen are the other interstitial elements present in these materials. The total effect of these three elements can be related through a parameter referred as the equivalent oxygen content O*, (O*=O+2N+2/3C wt.%)[32]. This parameter has values of 0.17% and 0.23% for the grade 2 and grade 3 titanium, respectively, used in this study. Thus we might in general expect an increase in interstitial content to decrease solubility and diffusion, just by the simple fact that more interstitial sites are occupied and not available for hydrogen.

The first consideration is whether composition differences can affect hydrogen diffusion. Hydrogen diffusion in α-titanium is very slow at temperatures below 80°C[20,28]. Although the hydrogen diffusion rates that we measured for the low purity and the high purity samples were different, this small difference cannot explain the difference in the mechanical test results. We can understand this point in the following way. The hydrogen diffusion distance, X, in a given time period, t, can be calculated as $X=\sqrt{Dt}$. If we assume that the diffusion coefficient in our experiments lies between 10^{-10} and 10^{-11} cm^2/s, we find that the penetration distance in one second ranges between 10^{-4} to $3x10^{-5}$ mm. If we make a rough estimate of the crack growth rate in our tests by simply dividing the gauge width by the time of the test, we find that at the slower crosshead speeds, crack propagation would not be diffusion limited in either grade 2 or grade 3. Thus we cannot attribute the different behavior of these two materials to differences in hydrogen diffusion.

The second possibility that we wish to consider is whether or not the solubility of hydrogen differs between the two grades of material. First, we note that our results which show hydrides in the interior of grade 3 would suggest that the solubility of hydrogen is lower in this material. Other research has also shown that the solubility of hydrogen in titanium varies

between 20 and 200 ppm in titanium alloys and that oxygen lowers the solubility of hydrogen[33,36]. Other elements can also change hydrogen solubility. For example, work by Pound indicated that high purity titanium would not absorb measurable amounts of hydrogen after electrolytic charging, while substantial hydrogen absorption was detected in commercial purity grade 2 titanium[37]. He explained that, in the case of grade 2 titanium, interstitial nitrogen appeared to be the principal irreversible trap at low hydrogen levels. Iron also affected hydrogen absorption in titanium[38]. Thus, we conclude that the reason why hydrides formed in the interior of grade 3 titanium and not grade 2 was that the solubility of hydrogen was lower in grade 3.

We now wish to consider the mechanics of crack propagation. Figures 53 and 54 show the appearance of the crack tip for grade 2 and grade 3 samples tested to point 1 in Figure 4 in 6%NaCl solution at a potential of -1400 mV_{SCE}. No microcracks could be observed in the crack tip area for grade 2 titanium. However, many microcracks or voids could be observed in grade 3 ahead of the crack tip. Examples can be seen in areas marked A, B, C, D and E. Closely spaced microcracks could connect with one another (for example at sites a and b) and those microcracks oriented near the crack tip joined with it to produce crack propagation. The cracks at sites A and B at high magnification appeared to be a result of cleavage cracking. Site F shows a void already connected to the main crack that would probably appear as a secondary crack on the fracture surface. Only the voids ahead of the crack tip connected with the crack tip and resulted in crack propagation. Other voids, such as those at sites D and E would not able to connect to the main crack; even if these voids were able to connect to the main crack they would not have contributed to further development of the crack since the stress concentration at these sites was not as high as that ahead of the main crack tip. Figure 55 shows collinear voids that were unable to connect with each other and with the crack because they were not ahead of the crack tip. In order to confirm these observations at the crack tip in grade 3 titanium samples, another test was performed. Figure 56 shows the appearance of the crack tip for a sample in 6%NaCl solution at a potential of -1400 mV_{SCE} after being tested in tension to point 2, as shown in Figure 4.

Based on the above results and discussion, a model describing the crack propagation for grade 2 and grade 3 titanium in 6%NaCl solution is proposed and shown in Figure 57. An explanation of this model is as follows.

(1.) Hydrogen atoms enter the area around the crack tip and form hydrides. Because of the volume change associated with the growing hydride[44], the area in front of the crack tip is a favored place for hydride nucleation, and the stress field associated with the growing hydride will eventually add to that of the crack tip.

(2.) Yielding occurs at the crack tip as a result of the applied stress. The crack tip becomes blunted and plastic slip occurs. This stress field will tend to nucleate voids at particles ahead of the crack tip, and since the hydrides are already stressed, they are ideal places for such voids to form. If hydrides have not precipitated, then much more deformation will be required to cause crack growth in these materials.

(3.) Voids around the crack tip grow and eventually connect up with the growing crack. The crack advances and then these steps are repeated.

(4.) If hydrides do not form in front of the crack tip, the entire process must take place by mechanical advance of the crack. Since grade 2 titanium does not have a high density of precipitates that will act as sites for void nucleation, we would expect extensive plastic deformation to accompany the cracking process. This deformation gives rise to the extensive elongation observed ahead of the crack tip. In contrast grade 3 does have hydrides ahead of the crack tip which could act as void nucleating sites in this process and would allow this mechanism to occur.

One final note should be made regarding the difference in susceptibility between grade 2 and grade 3 titanium. Because of the increased presence of interstitials, grade 3 titanium has a significantly higher yield strength than grade 2 titanium. Increased yield strength usually increases the susceptibility to hydrogen embrittlement because it allows for a sharp crack to be maintained more easily. This difference, coupled with the presence of brittle hydrides in the interior of grade 3, should greatly enhance cracking susceptibility.

5.0 CONCLUSIONS

1. The corrosion potential and cathodic reaction rate increased with decreasing pH and increasing temperature. Material and solution compositions had only small effects on the corrosion potential and cathodic reaction rates. However, heat treating the samples had a significant effect on this behavior.

2. The corrosion potential changed when titanium was galvanically coupled with other metals. Zinc and aluminum always cathodically polarized titanium. HY80 steel cathodically polarized titanium at temperatures above 50°C, but it anodically polarized titanium at room temperature. No hydrides could be detected in the Ti-HY80 couple after long time exposure in solution at room temperature. However, hydrides were detected in Ti-Al and Ti-Zn couples tested under the same conditions.

3. The critical potential for hydride formation was determined under various testing conditions. The potential increased with decreasing pH values and increasing temperature. Changing the pH had a more significant effect than changing the temperature. A surface film could significantly lower the critical potential for hydride formation.

4. A continuous hydride film formed on the surface of grade 2 titanium in a pH=1 solution, and the growth rate of the hydride phase decreased with time. In the pH=7 solution, the hydride phase formed in a non-continuous manner and was much thinner for the same time of growth.

5. The diffusion coefficient for hydrogen in titanium was measured with an electrochemical method at 70°C. The value was 9.9×10^{-11} cm^2/s in a low purity titanium and 3.6×10^{-11} cm^2/s in a high purity sample.

6. Grade 2 titanium had a low susceptibility to hydrogen embrittlement, regardless of sample geometry, orientation with respect to the rolling plane, and environmental conditions. For grade 3 titanium, the susceptibility to hydrogen embrittlement increased with decreasing electrochemical potential and decreasing crosshead speed during tensile testing. The solubility of hydrogen was lower in grade 3 than in grade 2, primarily because of the higher interstitial content. This lower solubility caused precipitation of hydrides in the matrix as well as on the surface of the sample.

7. A model to describe crack propagation in titanium was proposed. It basically involves a crack advance mechanism in which the cracks nucleate around the hydrides that formed ahead of the growing crack which would then link up with the main crack. If these hydrides did not precipitate, then the crack would require a higher mechanical stress to propagate. The fact that

hydrides did form ahead of the crack tip for grade 3 titanium but not for grade 2 led to the greater susceptibility for hydrogen cracking of grade 3 material.

6.0 REFERENCES

1 A. Atrens, D. Mezzanotte, N. F. Fiore and M. A. Genshaw, Corrosion Science, **20**, 673 (1980).

2 M. A. V. Devanathan and Z. Stachurski, Proc. Roy. Soc. **A270**, 90 (1962).

3 M. A. V. Devanathan and Z. Stachurski, J. the Electrochem. Soc., **111**, 619 (1964).

4 J. O'M. Bockris and P. K. Subramanyan, J. Electrochem. Soc., **118**, 1114 (1971).

5 C. L. Briant, K. S. Kumar and Z. F. Wang, "Hydriding of titanium" *First Annual Report*, N00014-96-1-0272 (1996).

6 L. L. Shreir, *Corrosion*, Vol 1, 2nd ed, published by Newnes-Butterworths, England (1976).

7 D. A. Jones, *Principles and Prevention of Corrosion*, Macmillan Publishing Company, New York, (1992).

8 Z. A. Foroulis, Boshoku Gijutsu, **29**, 113 (1980).

9 L. C. Covington, Corrosion, **35**, 378 (1979).

10 T. Fukuzuku, K. Shimogori, H. Satoh, and F. Kamikabo, Desalination, **31**, 389 (1979).

11 H. Satoh, T. Fukuzuka, K. Shimogori, and H. Tanabe, "Hydrogen Pick Up by Titanium Held Cathodic in Sea Water", 2nd International Congress on Hydrogen in Metals, Paris, France, June 6-11, Paper 6A1, (1977).

12 T. Nosetani, "Experience of Welded Titanium Tubes in Air Cooling Zone of Surface Condensers", Sumitomo Light Metal Technical Reports, 15(3), July, (1974).

13 D. Hardie, in *Environment-Induced Cracking of Metals* (ed R. P. Gangloff and M. B. Ives), NACE-10, 347 (1990).

14 D. S. Shih, I. M. Robertson, and H. K. Birnbaum, Acta Metall., **36**, 111 (1988).

15 J. K. Gregory, and H. -G. Brokmeier, Mater. Sci. Eng., **A203**, 365 (1995).

16 D. J. Simbi, and J. C. Scully, Corrosion Science, **35**, 489 (1993).

17 J. R. B. Gilbert, Titanium & Tech, **2**, 1105 (1984).

18 R. W. Schutz, and J. S. Grauman, "Determination of Cathodic Protential Limits for Prevention of Titanium Tube Hydride Embrittlement in Salt Water", Corrosion-89, Paper No. 110, April 17-21, New Orleans.

19 P. Millenbach and M. Givon, J. the Less-Common Metals, **87**, 179 (1982).

20 I. I. Phillips, P. Poole and L. L. Shreir, Corrosion Science, **14**, 533 (1974).

21 J. B. C. Wu, "Effect of Iron Content on Hydrogen Absorption and Passivity Breakdown of Commercially Pure Titanium in Aqueous", 5th Inter. Conf. on Titanium Science and Technology, Oberusel (West Germany), 2559 (1985).

22 R. Otsuka, Sci. Papers I. P. C. R. **54**, 97 (1960).

23 N. Tomashov, V. N. Modestova and A. S. Anatolev'a, Corrosion of Metals and Alloys, Collection No. 1 (Ed. C. J. L. Booker, Trans. A. D. Mercer), N. L. L. S. T., Boston Spa, 207 (1964).

24 I. I. Phillips, P. Pool, and L. L. Shreir, Corrosion Science, **12**, 1972, p866.

25 D. T. Peterson and D. G. Westlake, J. Am. Chem. Soc., **64**, 649 (1960).

26 D. C. Carmichael, J. R. Hornaday, A. E. Morris and N. A. Parlee, Trans. Met. Soc., AIME, **218**, 826 91960).

27 E. Brauer, R. Dîrr and H. Z¸chner, Z. Phys. Chem. N. F., **100**, 109 (1976).

28 R. L. Jacobs, and J. A. McMaster, Materials Protection and Performance, **11**, 33 (1972).

29 O. S. Abdul-Hamid and R. M. latanision, "Hydrogen Effects in Materials", Ed: by A. W. Thompson and N. R. Moody, A Publication of TMS, 205 (1994).

30 S. Takano and T. Suzuki, Acta Metall., **22**, 265 (1974).

31 S. Gahr, M. L. Grossbeck and H. K. Birnbaum, Acta Metall, **35**, 125 (1977).

32 R. I. Jaffee, F. C. Holden, and H. R. Ogden. J. Metals Trans. AIME , 1282 (1954).

33 G. R. Caskey, Mater. Sci. Eng., **14**, 109 (1974).

34 A. Jostsons, and A. E. Jenkins, Trans. AIME, **239**, 1318 (1967).

35 S. Yamanaka, T. Tanaka, S. Tsuboi, and M. Miyake, Fusion Eng., **10**, 303 (1989).

36 T. H. Qyach-Kamimura, D. David, G. Beranger, A. Falanga, and G. Lozes, J. Less-Common Met., **125**, 59 (1986).

37 B. G. Pound, Corrosion, **47**, 99 (1991).

38 J. B. Cotton, Chemical Engineering Progress, **66**, 57 (1970).

39 S. Takano and T. Suzuki, Acta Metall. **22**, 265 (1974).

40 S. Gahr, M. L. Grossbeck and H. K. Birnbaum, Acta Metall., **35**, 125 (1977).

41 R. Dutton, N. Nuttall, M. P. Puls and L. A. Simpson, Metall. Trans., **8A**, 1553 (1977).

42 R. Dutton, C. H. Woo, K. Nuttall, L. A. Simpson and M. P. puls, 2nd Int. Conf. on Hydrogen in Metals, Pergamon Press. Oxford, Paper 3C6 (1977).

43 N. E. Paton and J. C. Williams, Hydrogen in Metals, edited by I. M. Bernstein and A. W. Thompson), Am. Soc. Metals, Metal Park, Ohio, 409 (1974).

44 D. S. Shih, I. M. Robertson and H. K. Birnbaum, Acta Metall., **36**, 111 (1988).

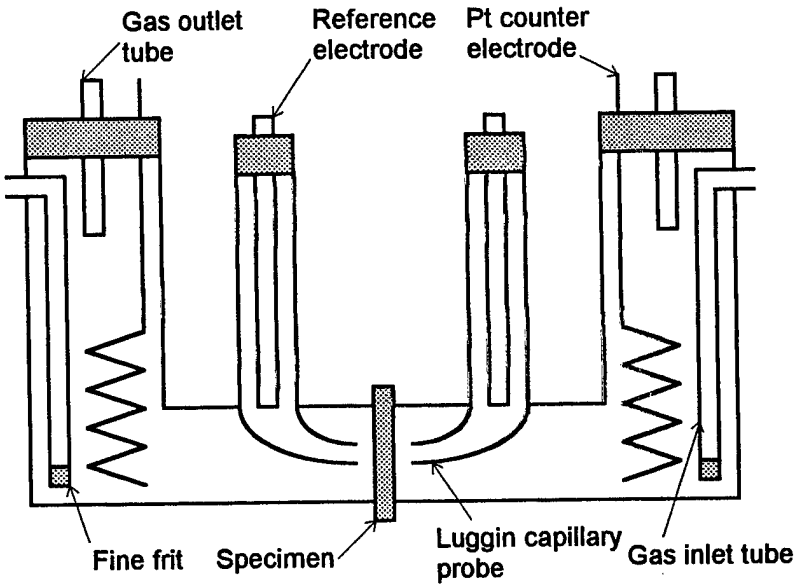

Figure 1 - Cell used for measuring hydrogen diffusion.

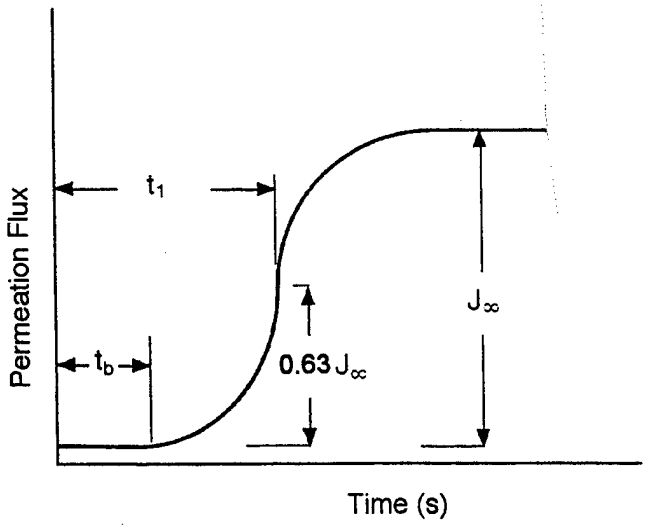

Figure 2 - Typical hydrogen permeation transient.

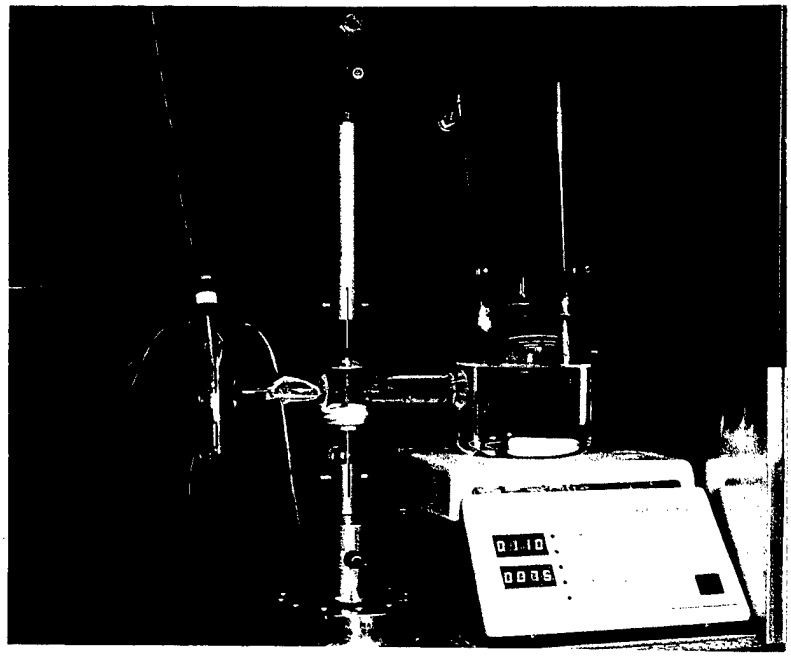

Figure 3 - Setup for mechanical tests.

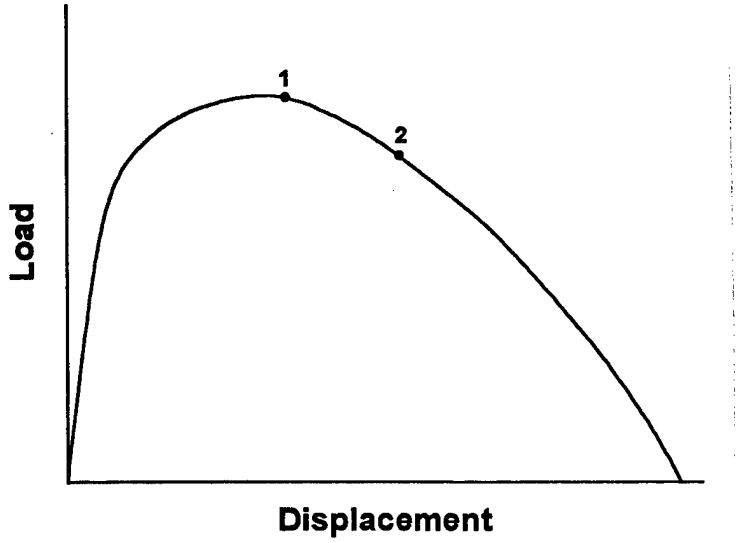

Figure 4 - Typical curve of load vs. displacement for notched sample.

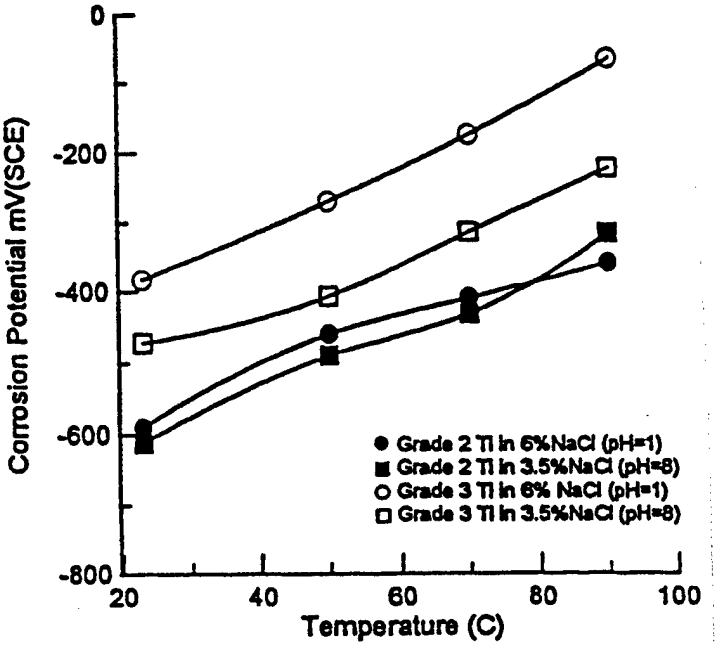

Figure 5 - The variation of the corrosion potential with temperature for grade 2 and grade 3 titanium in 3.5% and 6%NaCl solutions with different pH values.

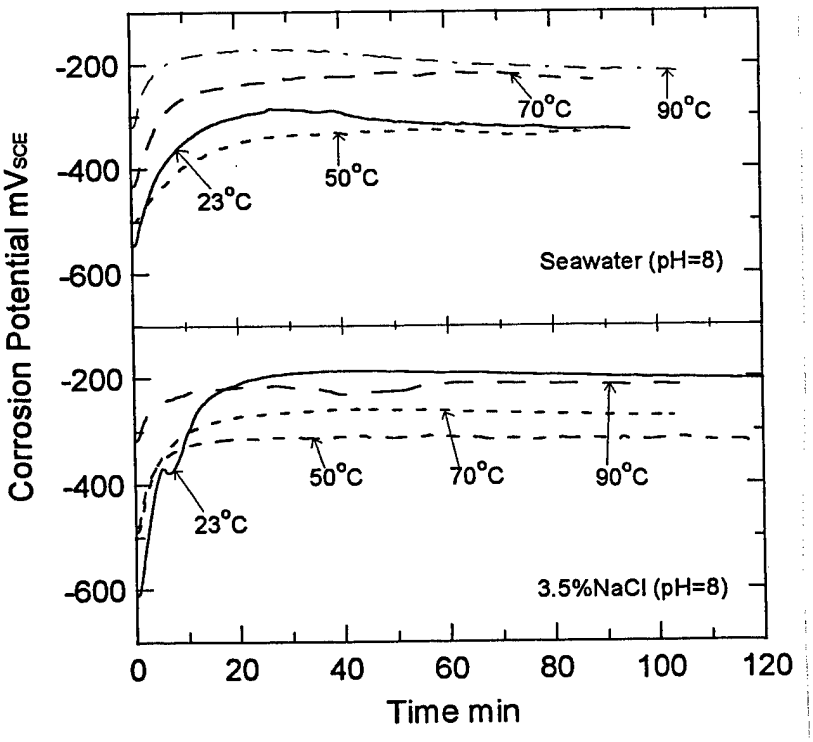

Figure 6 - The variation of the corrosion potential with time for grade 2 titanium in sea water (pH=8) and 3.5%NaCl solution (pH=8).

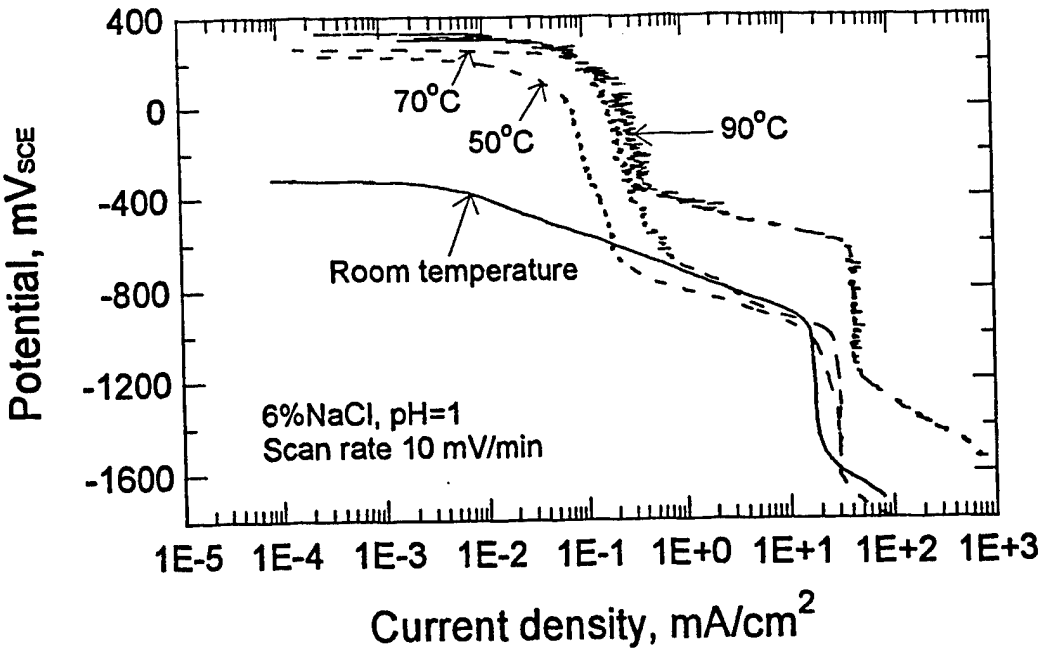

Figure 7 - Cathodic polarization curve at various temperatures for grade 2 titanium in 6%NaCl solution with pH=1.

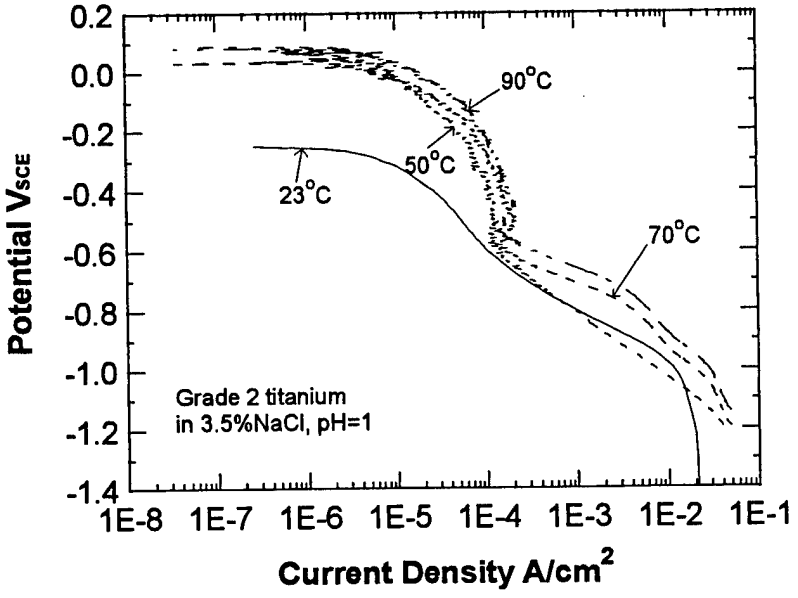

Figure 8 - Cathodic polarization curve at various temperatures for grade 2 titanium in 3.5%NaCl solution with pH=1.

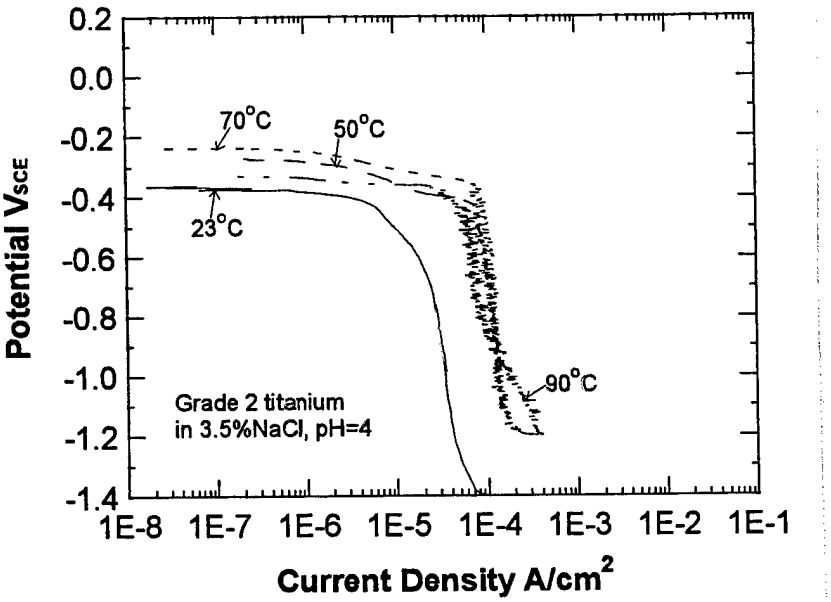

Figure 9 - Cathodic polarization curve at various temperatures for grade 2 titanium in 3.5%NaCl solution with pH=4.

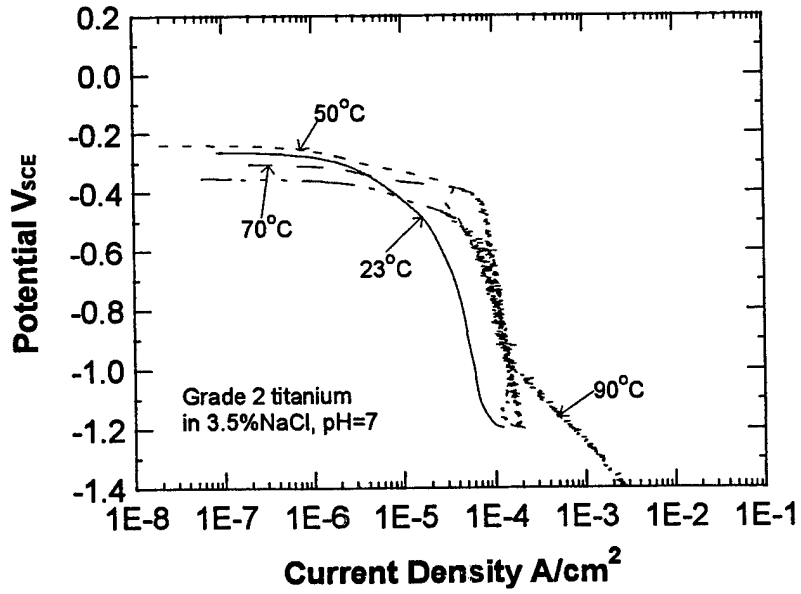

Figure 10 - Cathodic polarization curve at various temperatures for grade 2 titanium in 3.5%NaCl solution with pH=7.

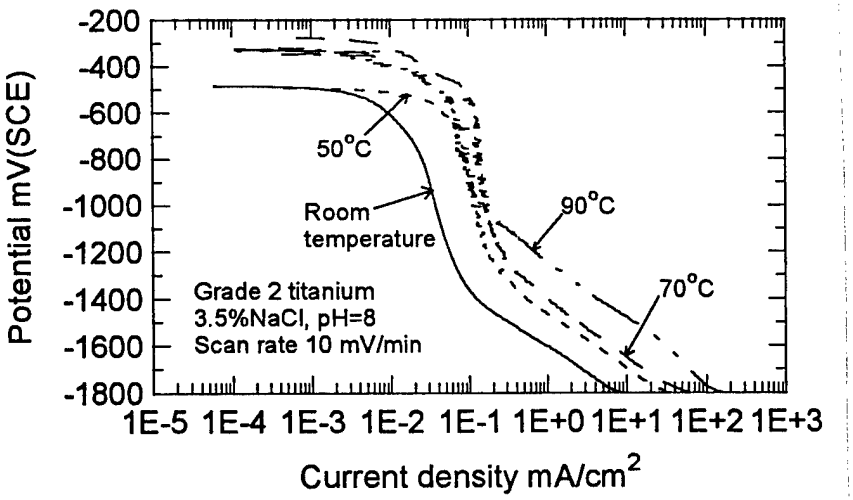

Figure 11 - Cathodic polarization curve at various temperatures for grade 2 titanium in 3.5%NaCl solution with pH=8.

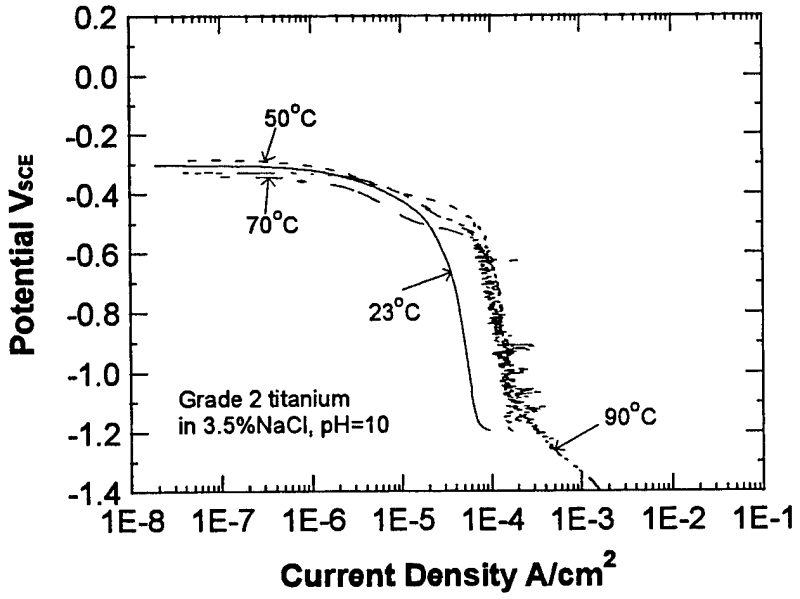

Figure 12 - Cathodic polarization curve at various temperatures for grade 2 titanium in 3.5%NaCl solution with pH=10.

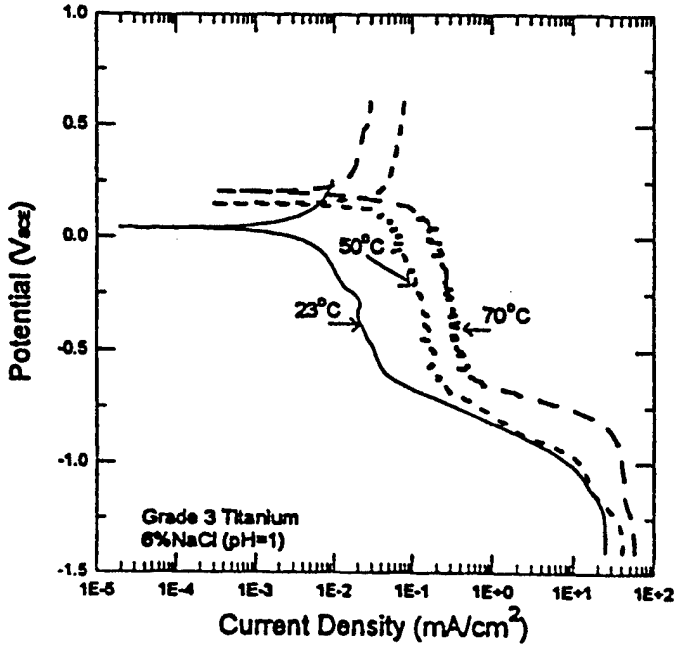

Figure 13 - Polarization curve for grade 3 titanium at various temperatures in 6%NaCl solution with pH=1.

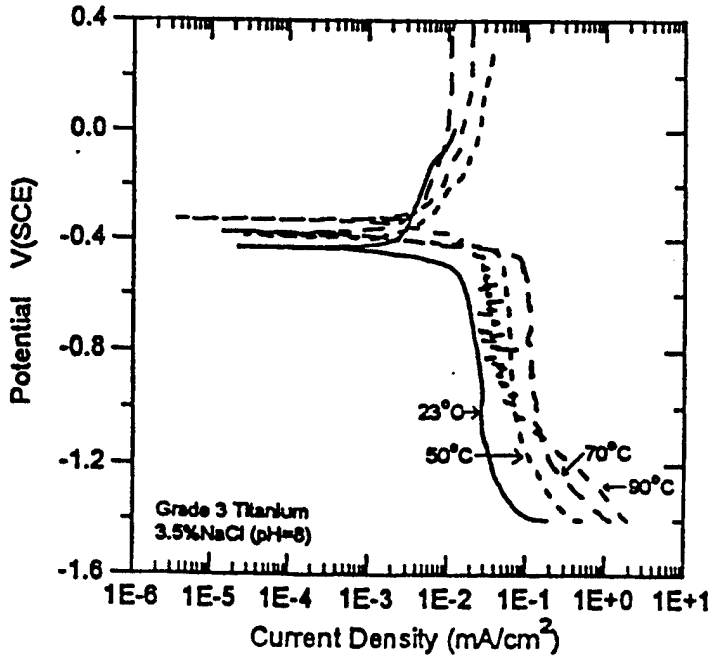

Figure 14 - Polarization curve for grade 3 titanium at various temperatures in 3.5%NaCl solution with pH=8.

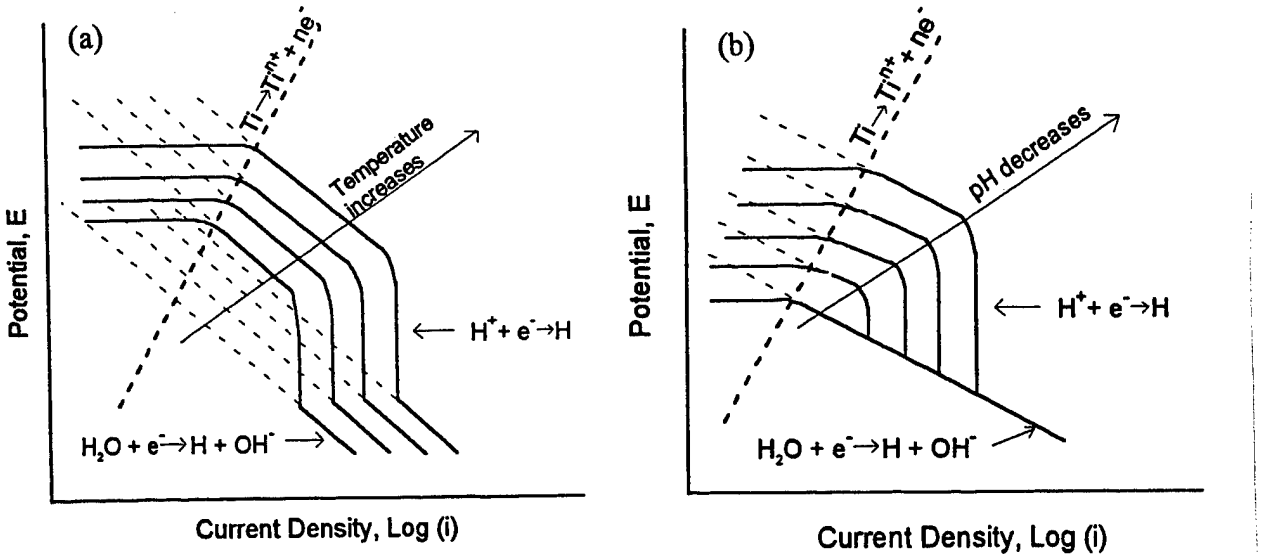

Figure 15 - Schematic illustration of the effect of temperature and pH on the corrosion potential and cathodic reaction rate in the absence of oxygen in solution, (a) temperature effect and (b) pH effect.

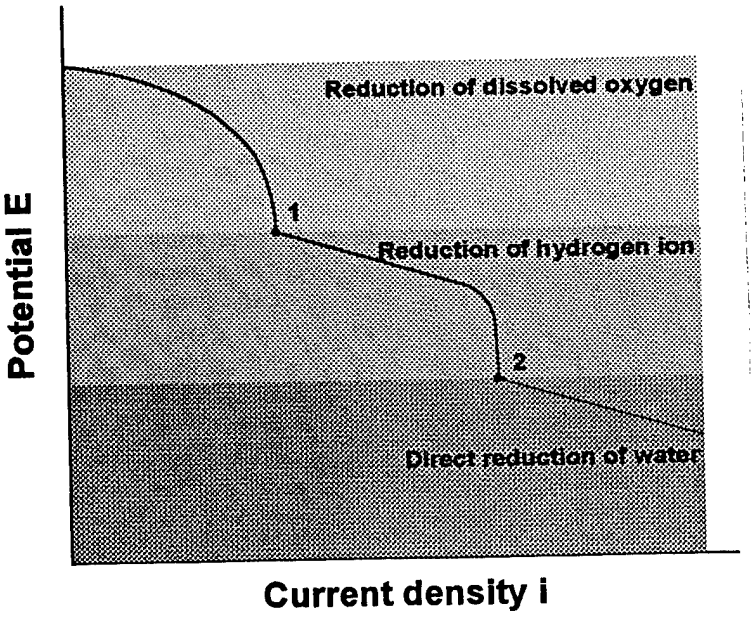

Figure 16 - Illustration of cathodic polarization curve with different cathodic reactions.

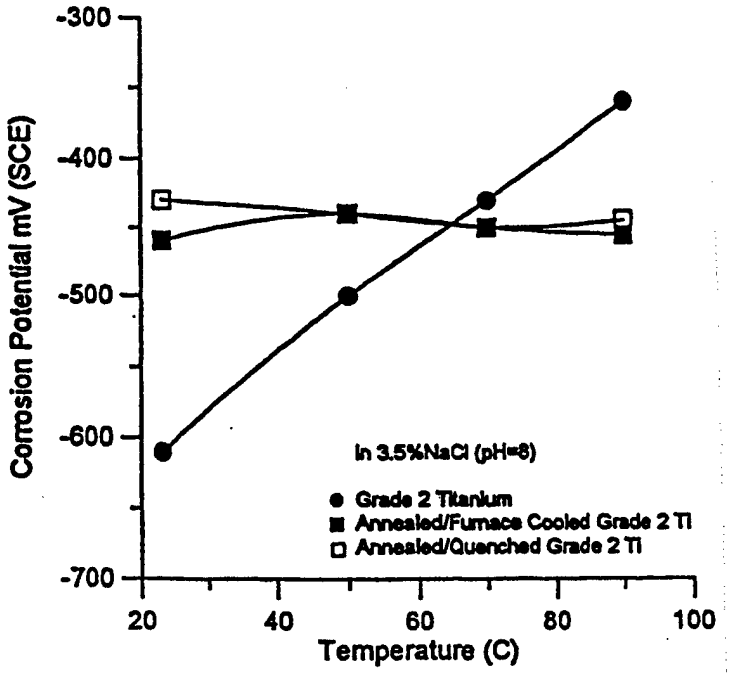

Figure 17 - The variation of the corrosion potential with temperature for heat-treated grade 2 titanium in 3.5%NaCl solution with pH=8.

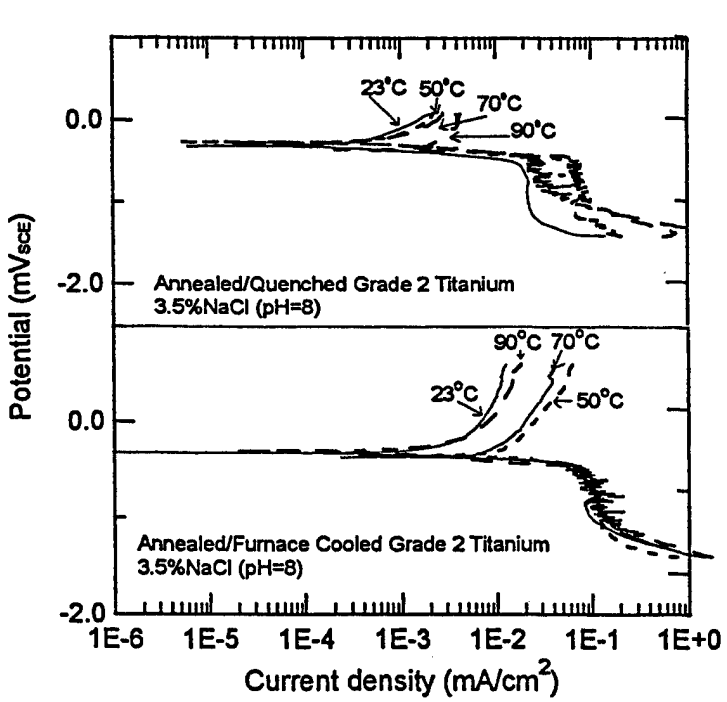

Figure 18 - Polarization curve for heat-treated grade 2 titanium at various temperatures in 3.5%NaCl solution with pH=8.

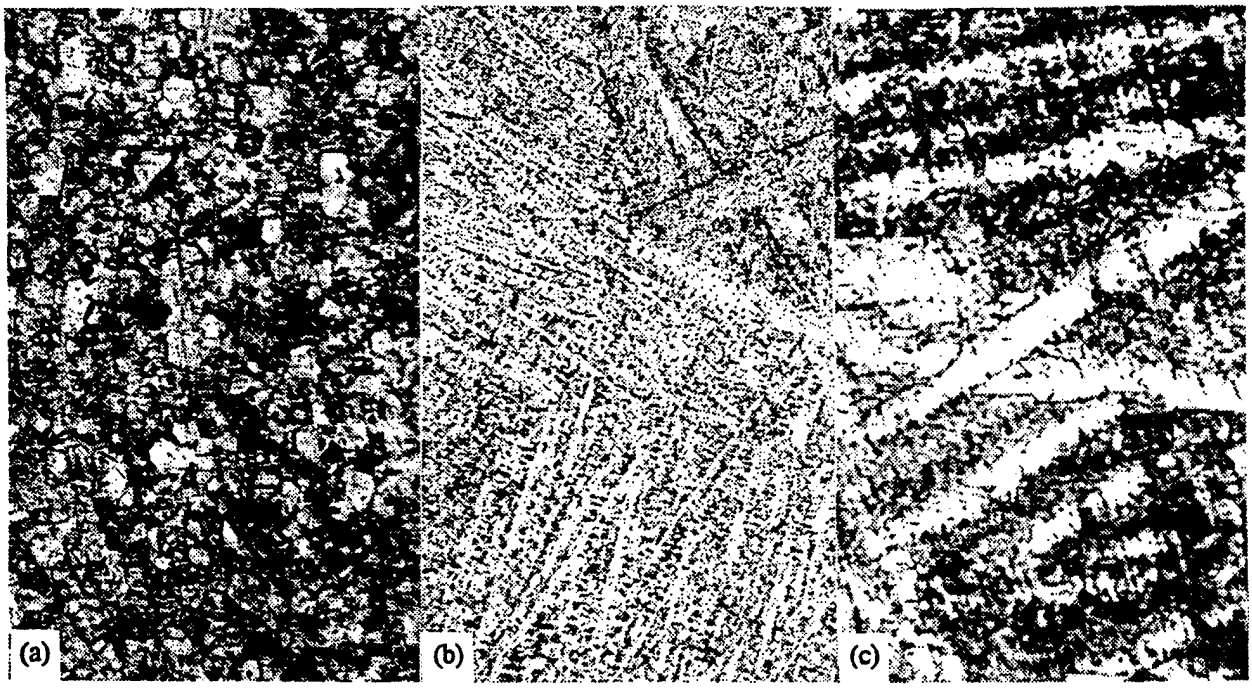

Figure 19 - Micrographs of (a) as-received, (b) annealed/water-quenched and (c) annealed/furnace-cooled grade 2 titanium.

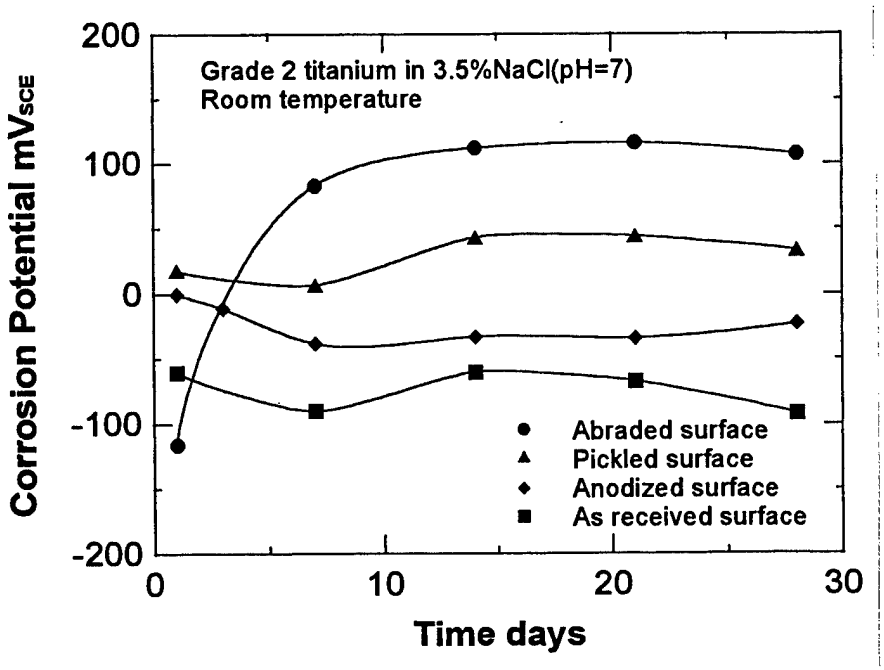

Figure 20 - The variation of the corrosion potential with time for grade 2 titanium samples with different surface conditions in 3.5%NaCl solution (pH=7) at room temperature.

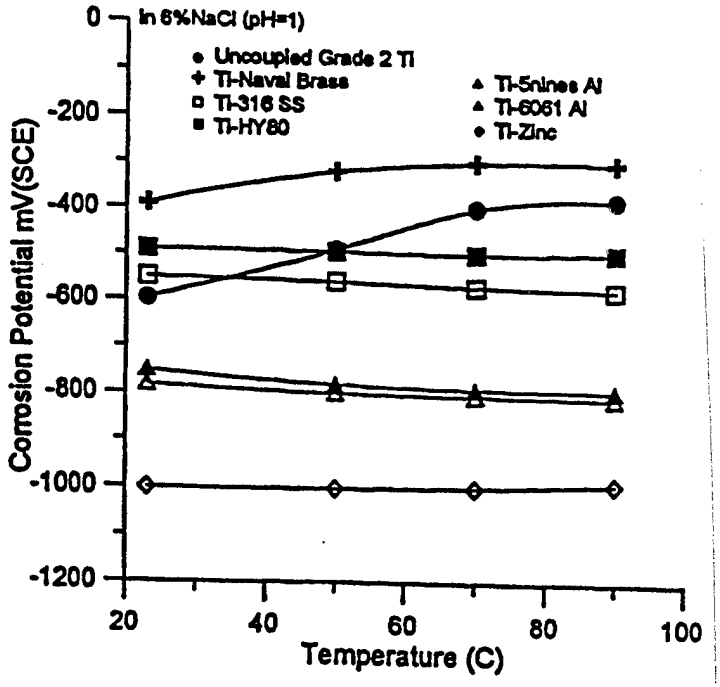

Figure 21 - The variation of the corrosion potential with temperature for grade 2 titanium coupled with other metals in 6%NaCl solution with pH=1.

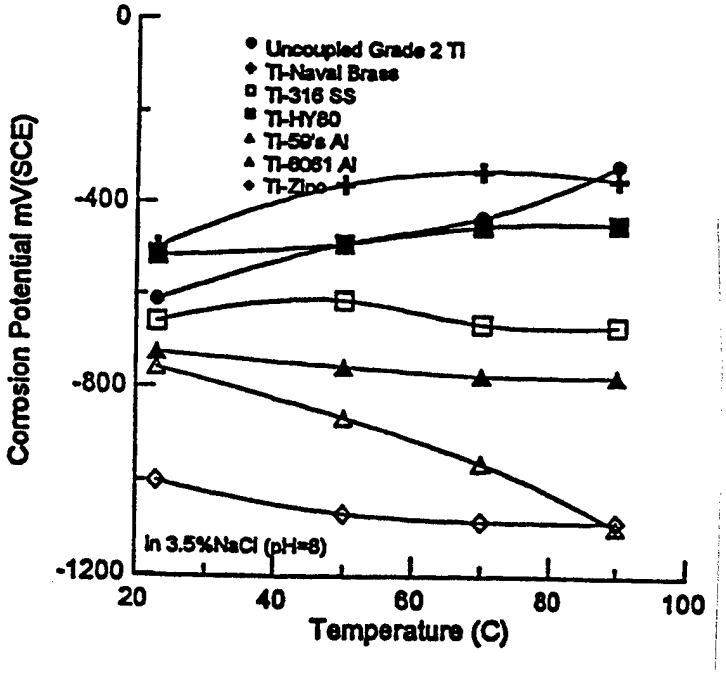

Figure 22 - The variation of the corrosion potential with temperature for grade 2 titanium coupled with other metals in 3.5%NaCl solution with pH=8.

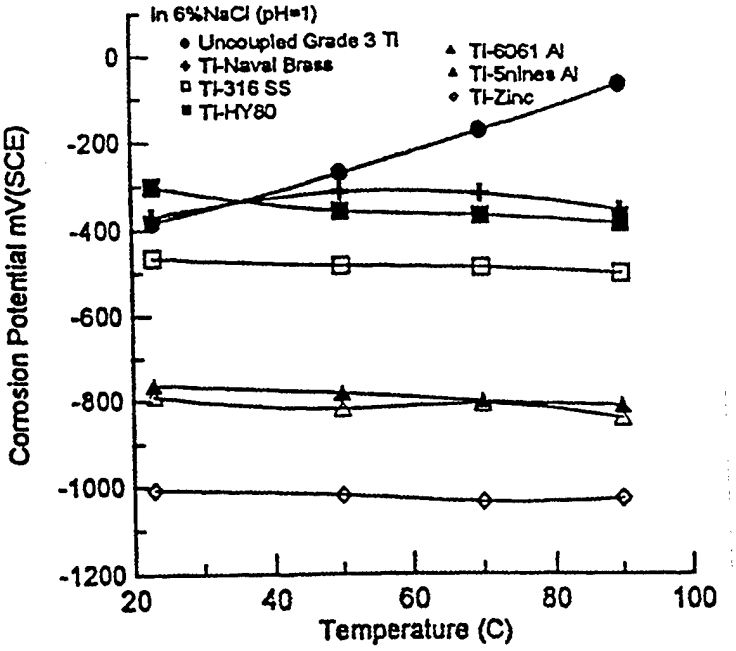

Figure 23 - The variation of the corrosion potential with temperature for grade 3 titanium coupled with other metals in 6%NaCl solution with pH=1.

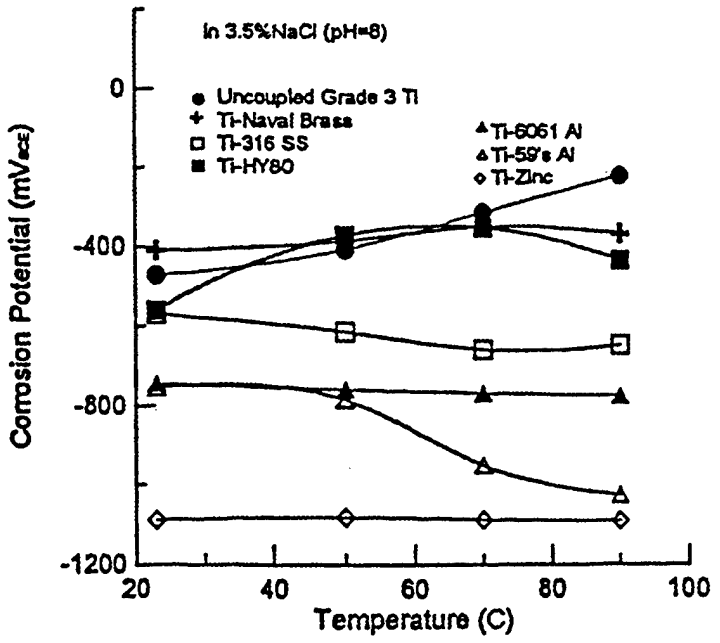

Figure 24 - The variation of the corrosion potential with temperature for grade 3 titanium coupled with other metals in 3.5%NaCl solution with pH=8.

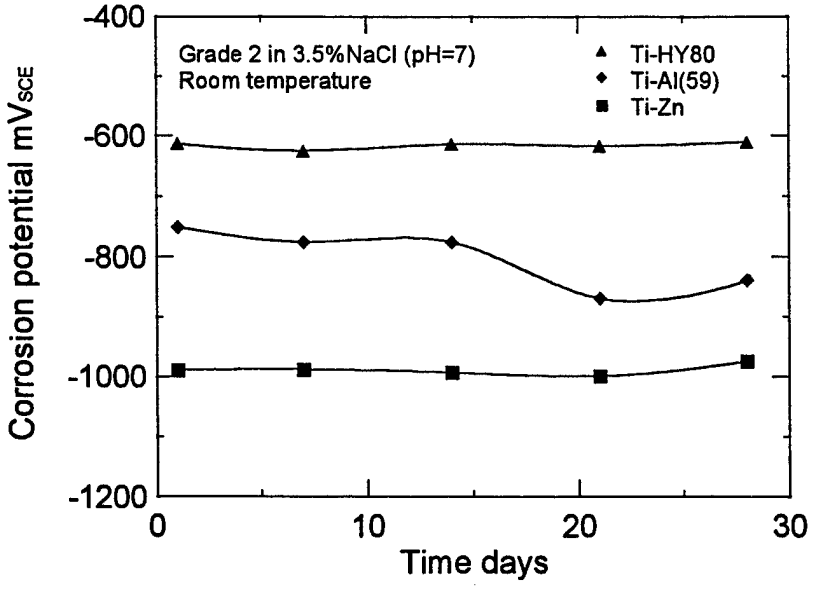

Figure 25 - The variation of the corrosion potential with time for grade 2 titanium coupled with other metals in 3.5%NaCl solution (pH=7) at room temperature.

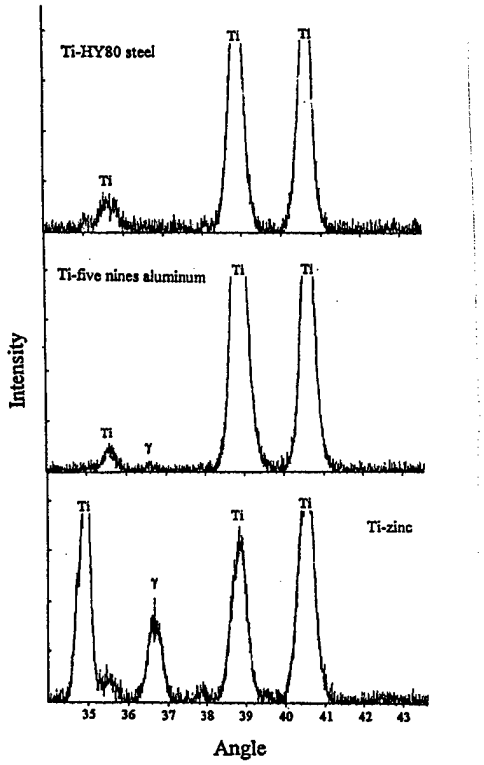

Figure 26 - XRD pattern obtained from grade 2 titanium coupled with HY80 steel, five-nines aluminum, and zinc after being exposed in 3.5%NaCl (pH=8) solution at room temperature for four weeks.

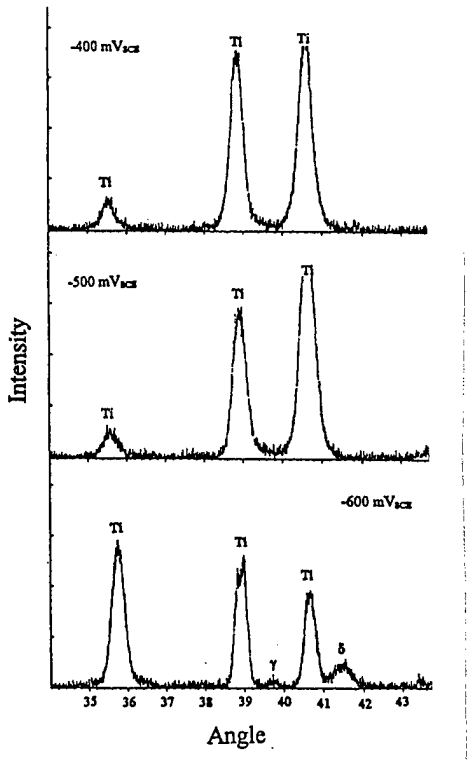

Figure 27 - XRD pattern obtained from grade 2 titanium samples after being charged at different potentials in 3.5%NaCl solution (pH=1) at 90°C for 24 hours.

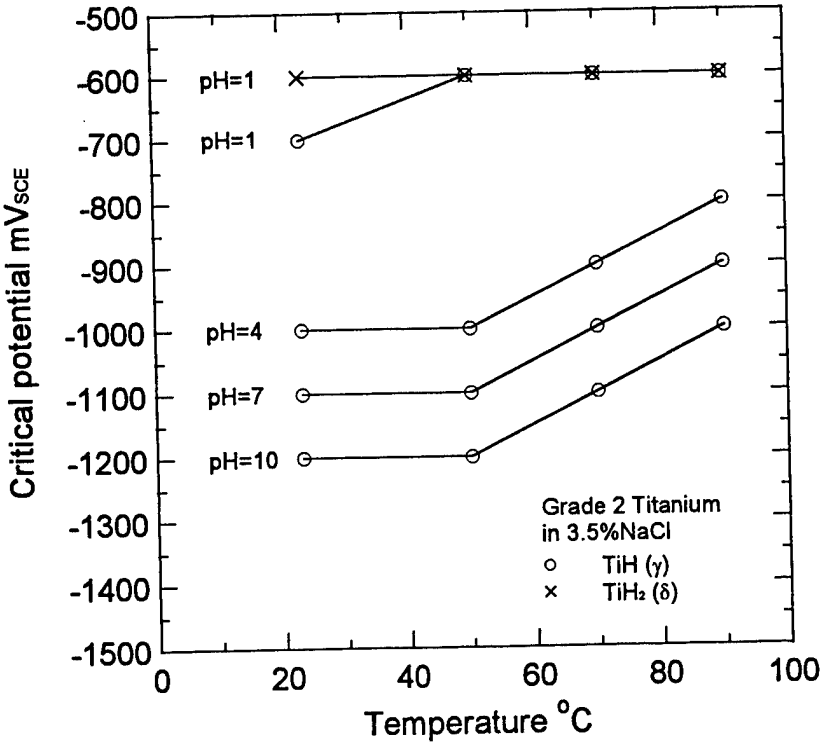

Figure 28 - The critical potential of hydride formation as a function of temperature and pH value for grade 2 titanium in 3.5%NaCl solution.

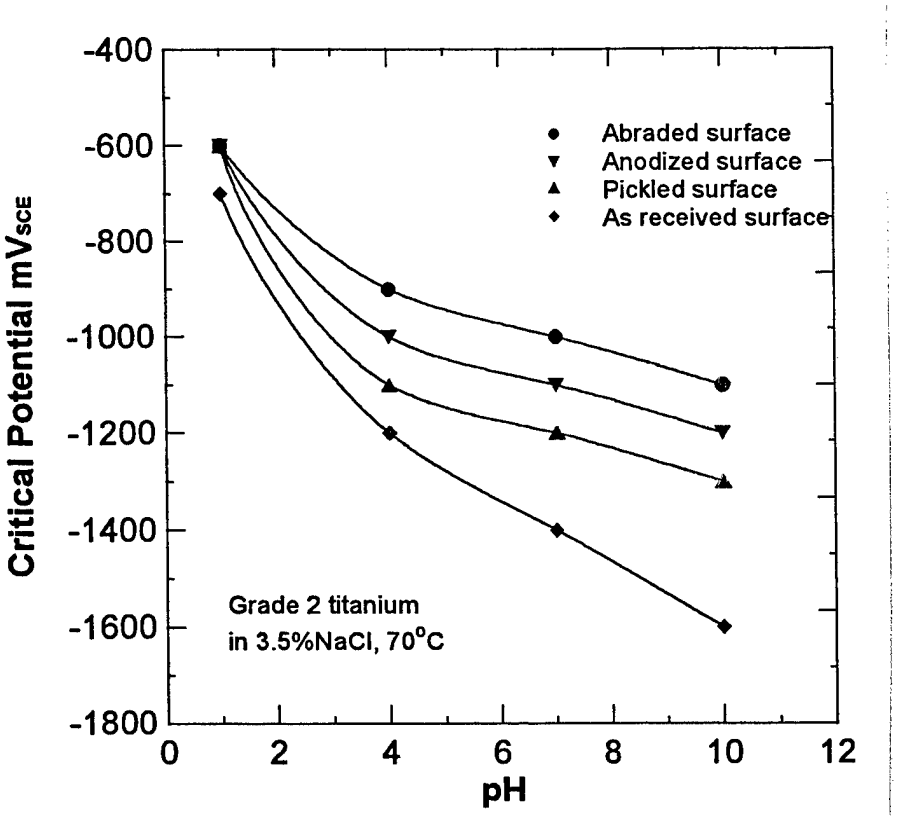

Figure 29 - The critical potential of hydride formation as a function of pH value for grade 2 titanium with different surface conditions in 3.5%NaCl solution at 70°C.

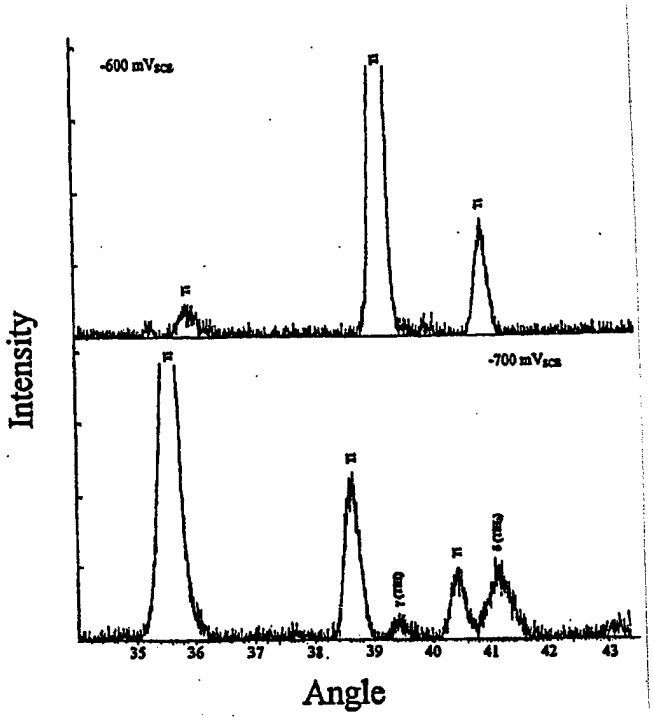

Figure 30 - XRD pattern obtained from grade 3 titanium samples after being charged at a potential of -600 and -700 mV$_{SCE}$ in 6%NaCl solution (pH=1) at 70°C for 24 hours.

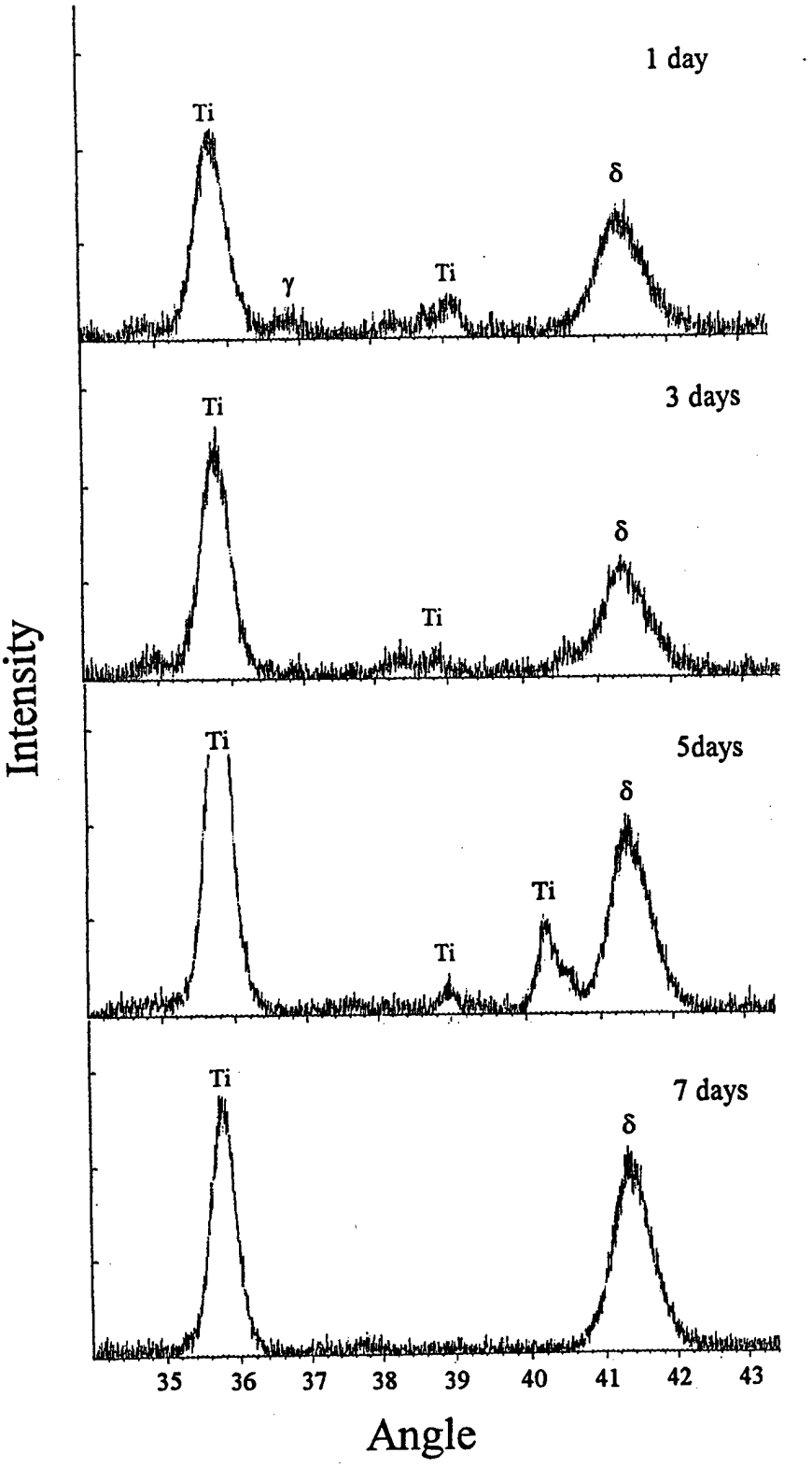

Figure 31 - XRD pattern obtained from grade 2 titanium samples after being charged at a potential of -1400 mV_{SCE} in 3.5%NaCl solution (pH=1) at 70°C for up to 168 hours.

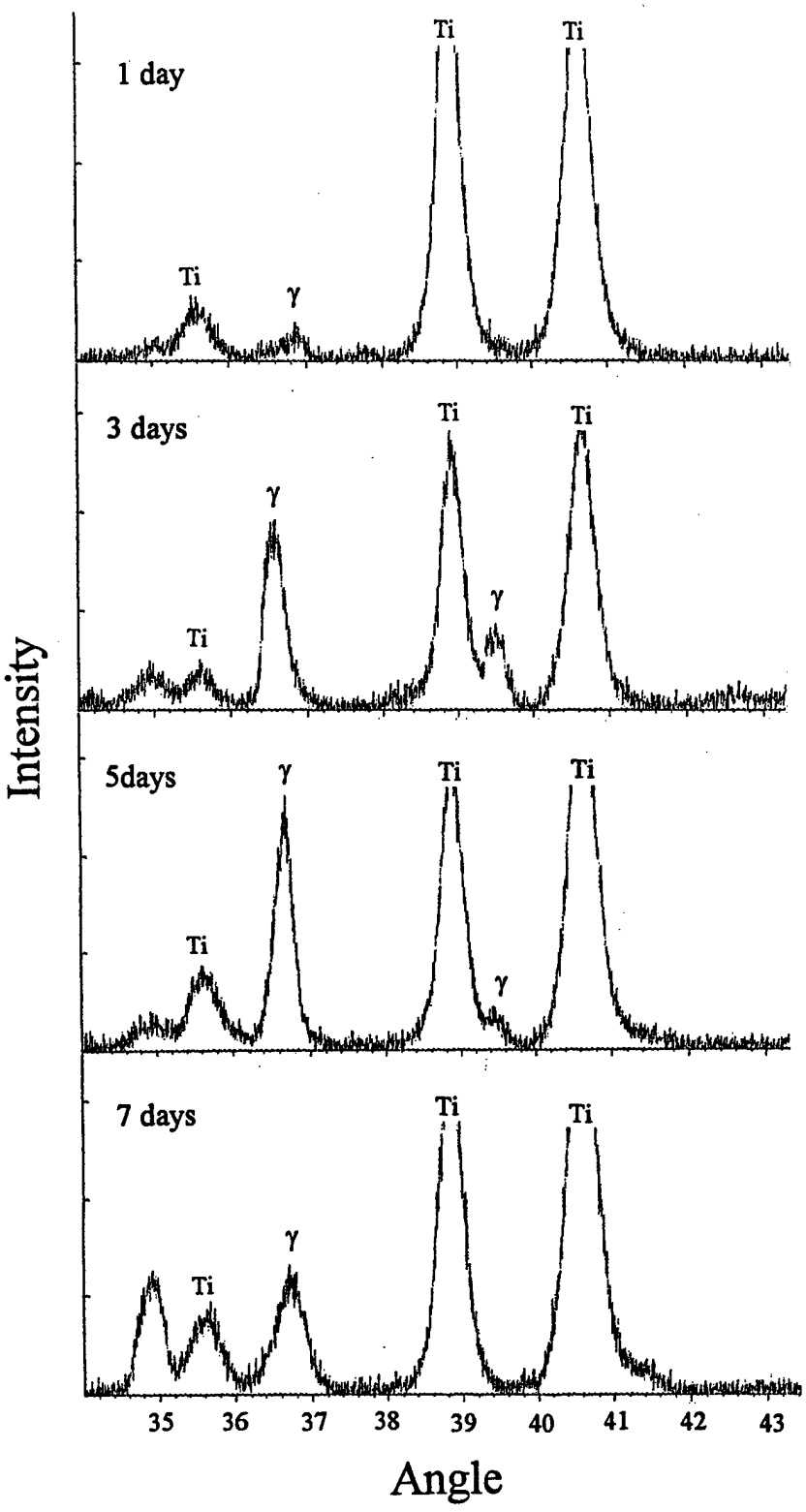

Figure 32 - XRD pattern obtained from grade 2 titanium samples after being charged at a potential of -1400 mV_{SCE} in 3.5%NaCl solution (pH=7) at 70°C for up to 168 hours.

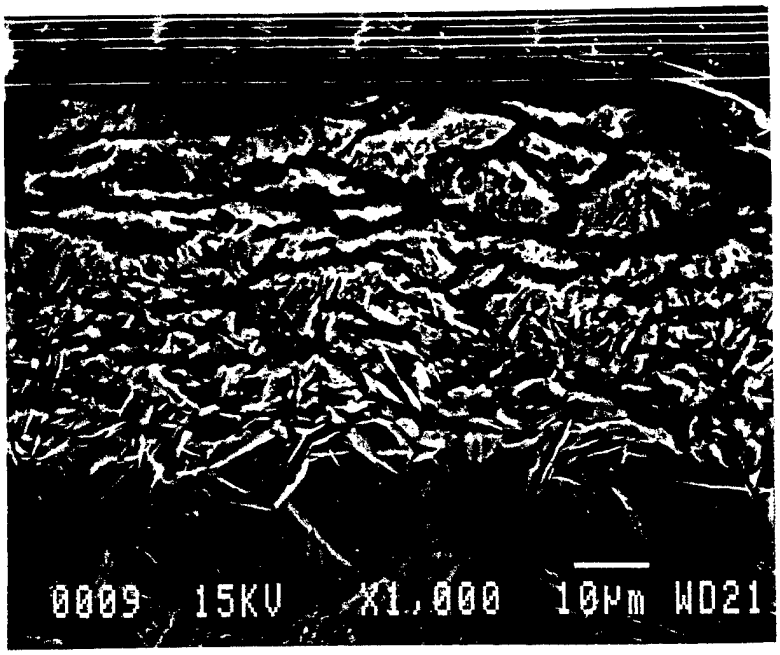

Figure 33 - Microstructure of hydride layer on the grade 2 titanium sample surface after the sample was charged in 3.5%NaCl solution (pH=1) at -1400 mV_{SCE} and 70°C for 168 hours.

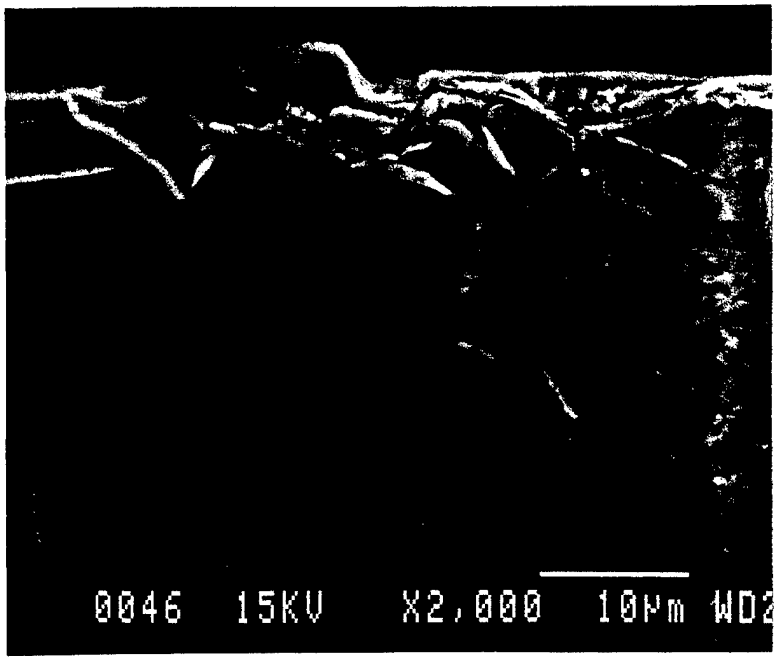

Figure 34 - Microstructure of hydride layer on the grade 2 titanium sample surface after the sample was charged in 3.5%NaCl solution (pH=1) at -1400 mV_{SCE} and 70°C for 168 hours.

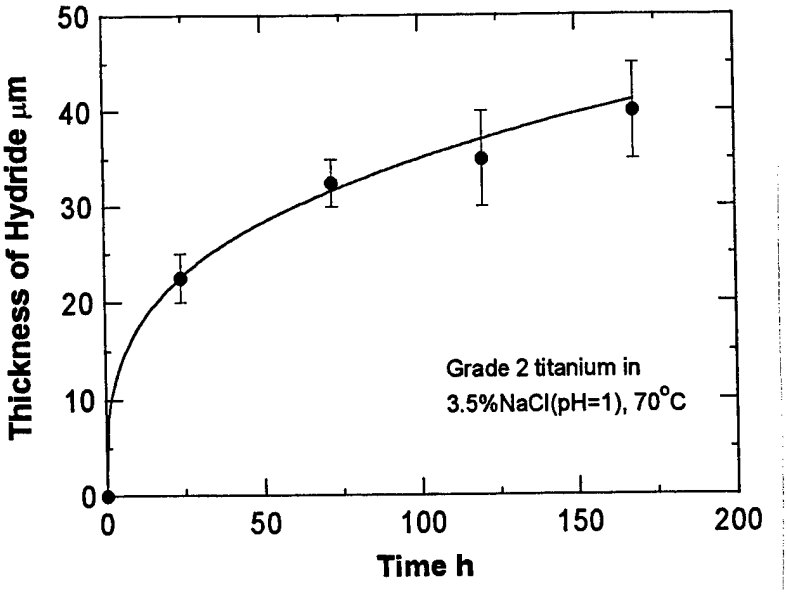

Figure 35 - The thickness of the hydride layer on the grade 2 titanium sample as a function of charging time in 3.5%NaCl solution (pH=1) at -1400 mV_{SCE} and 70°C.

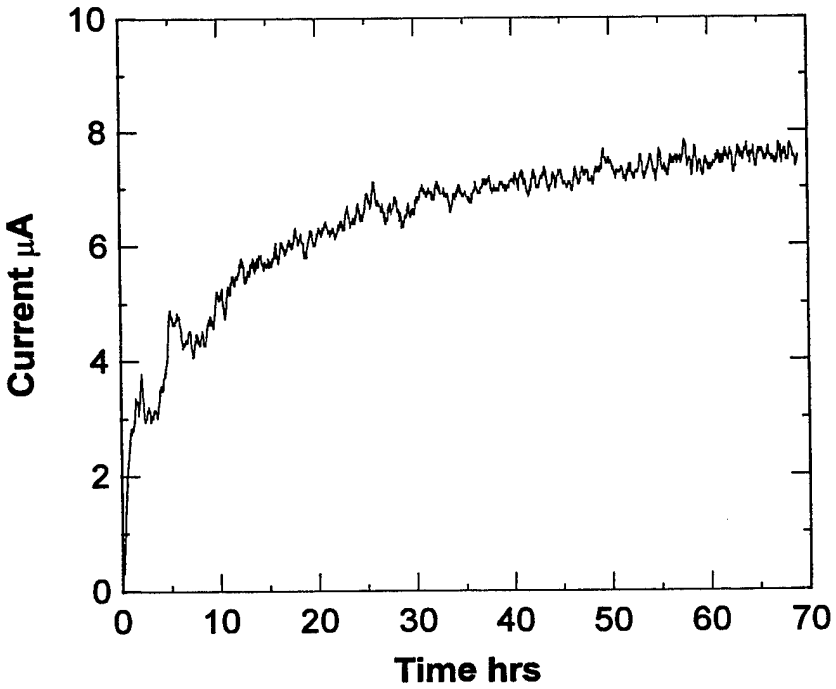

Figure 36 - Hydrogen permeation current plotted as a function of time for the LP sample with pickled surface at -1500 mV_{SCE}.

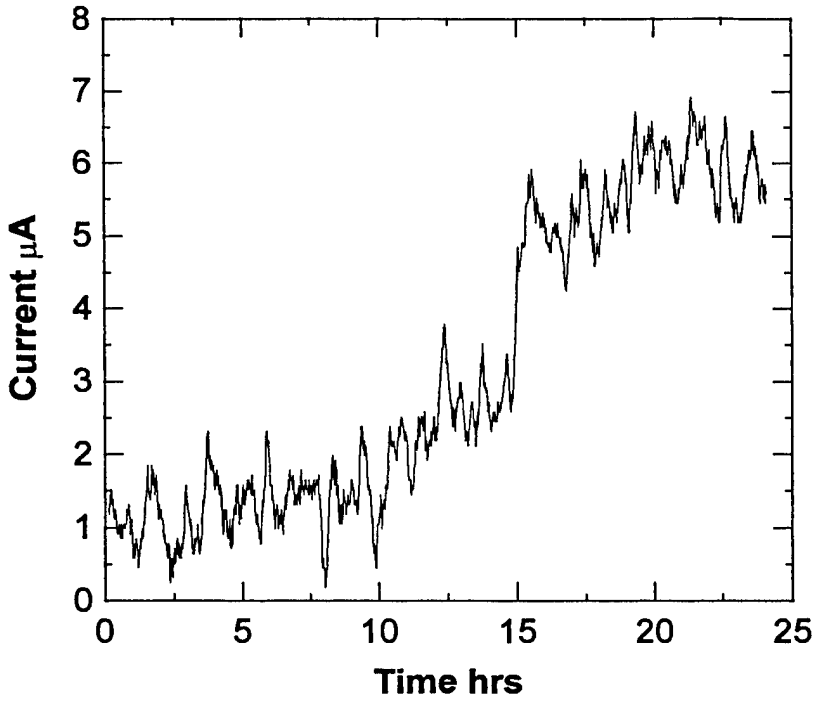

Figure 37 - Hydrogen permeation current plotted as a function of time for the LP sample with pickled surface at -1800 mV_{SCE}.

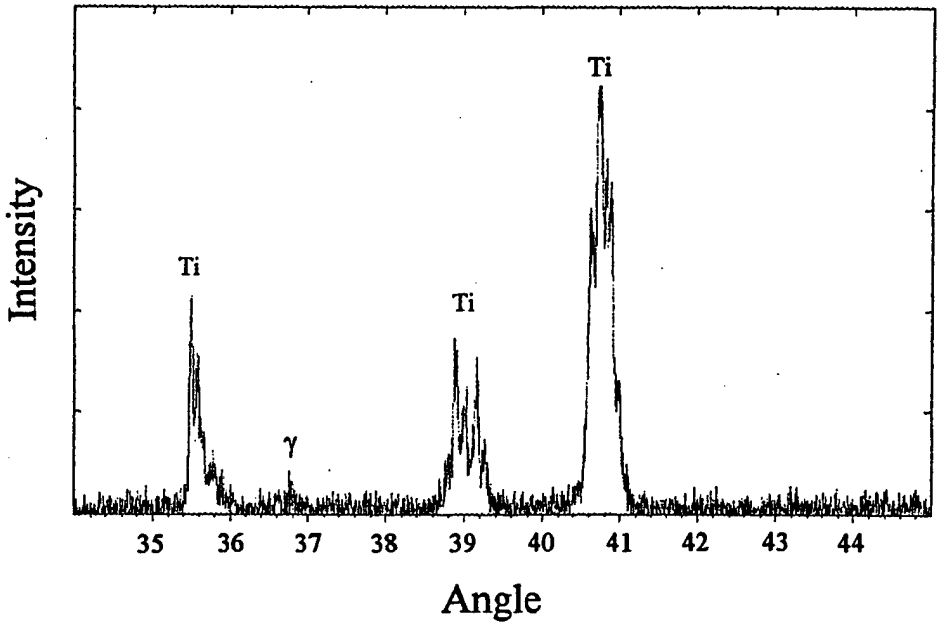

Figure 38 - XRD pattern obtained from LP samples with pickled surface after being charged at a potential of -1800 mV_{SCE}.

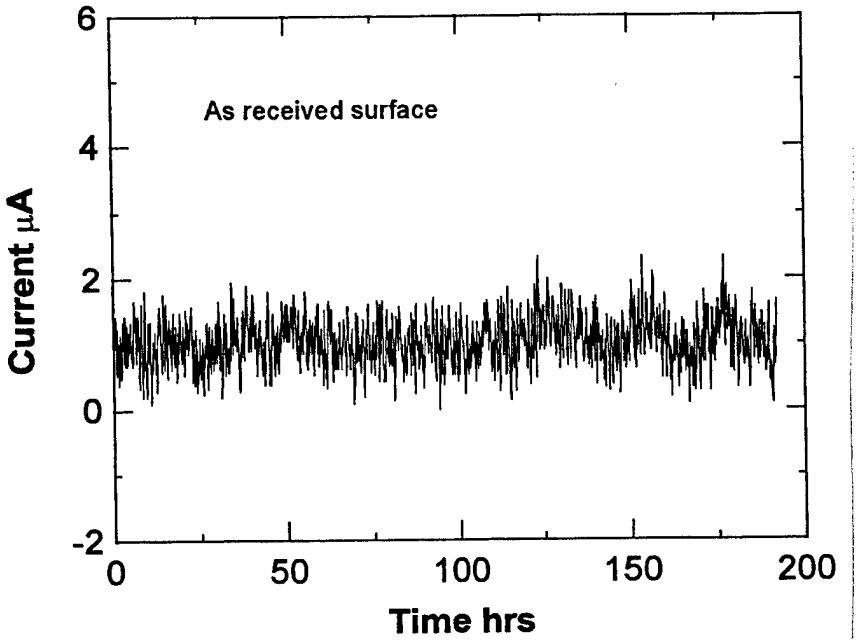

Figure 39 - Hydrogen permeation current plotted as a function of time for the LP sample with the as-received surface at -1500 mV_{SCE}.

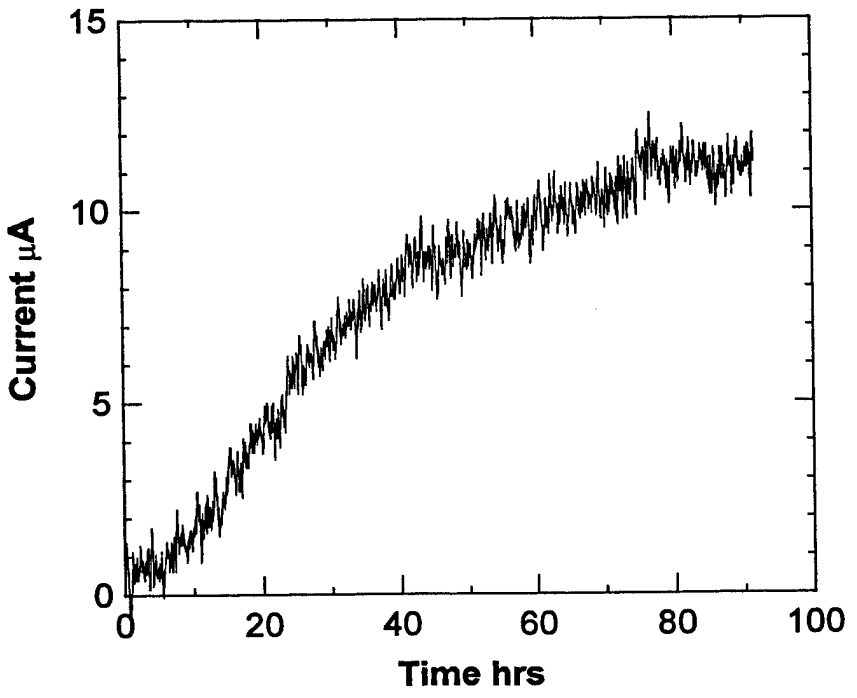

Figure 40 - Hydrogen permeation current plotted as a function of time for the HP sample with a pickled surface at -1500 mV_{SCE}.

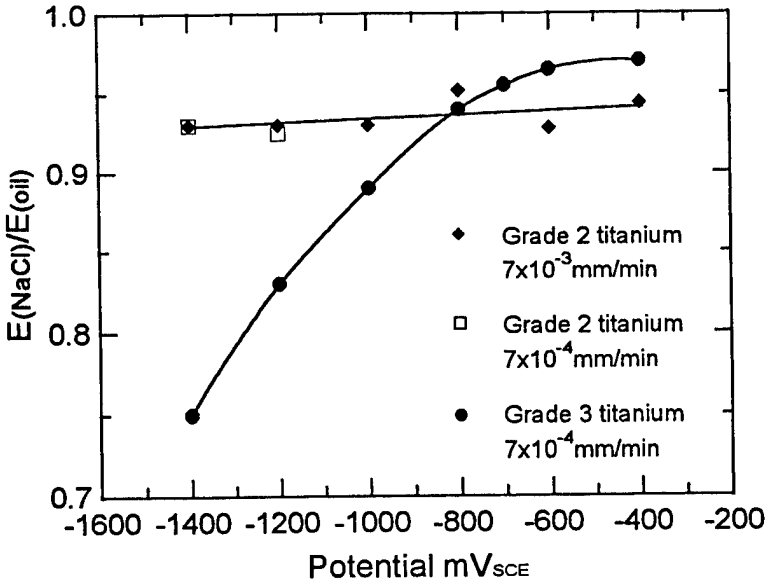

Figure 41 - The ratio of the elongation to failure in 6%NaCl (pH=1) to that obtained in oil plotted as a function of applied potential for grade 2 and grade 3 titanium at 70°C.

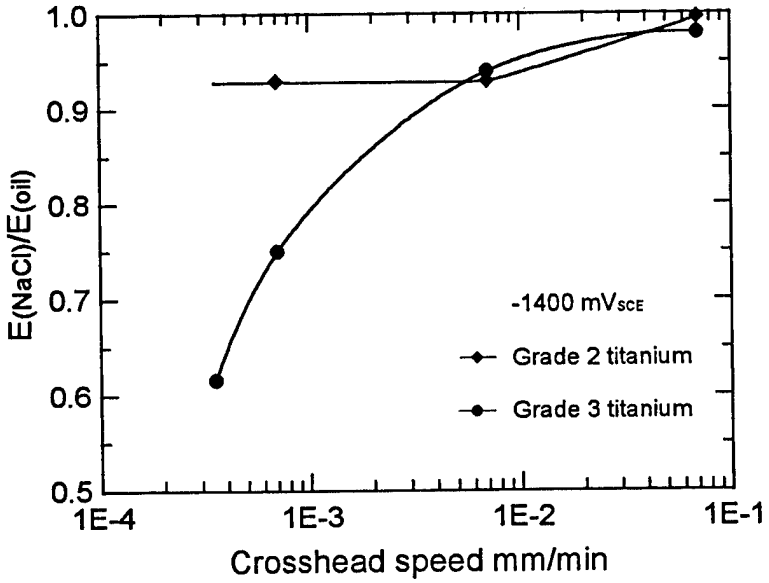

Figure 42 - The ratio of the elongation to failure in 6%NaCl (pH=1) to that obtained in oil plotted as a function of applied crosshead speed for grade 2 and grade 3 titanium at 70°C.

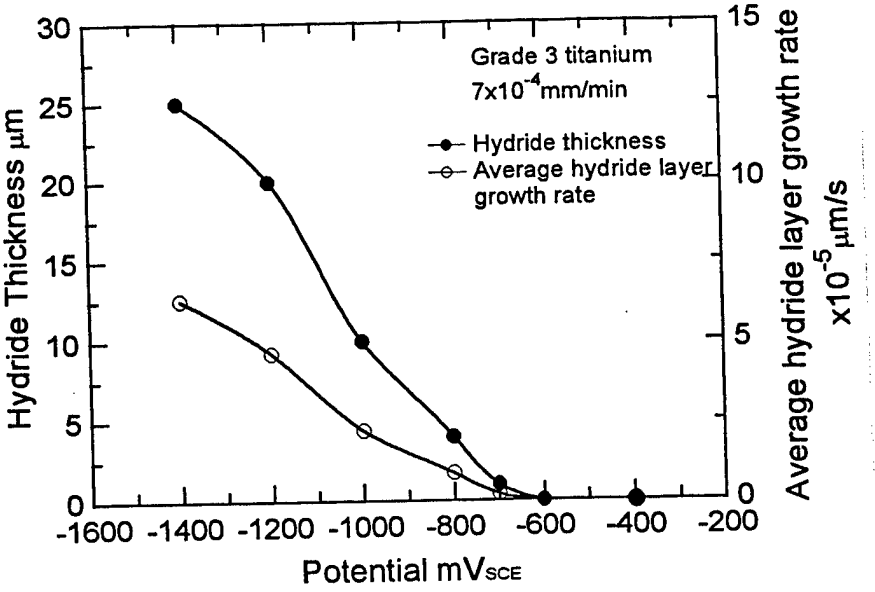

Figure 43 - Effect of applied potential on the thickness of the hydride layer and average hydride layer growth rate on grade 3 titanium surface in 6%NaCl (pH=1) at 70°C.

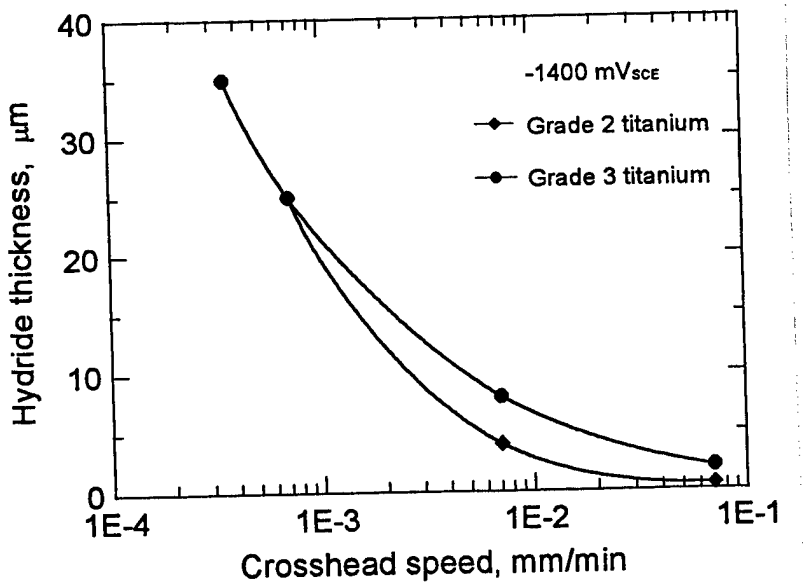

Figure 44 - Effect of applied crosshead speed on the thickness of the hydride layer on grade 2 and grade 3 titanium surface at -1400 mV_{SCE} at 70°C.

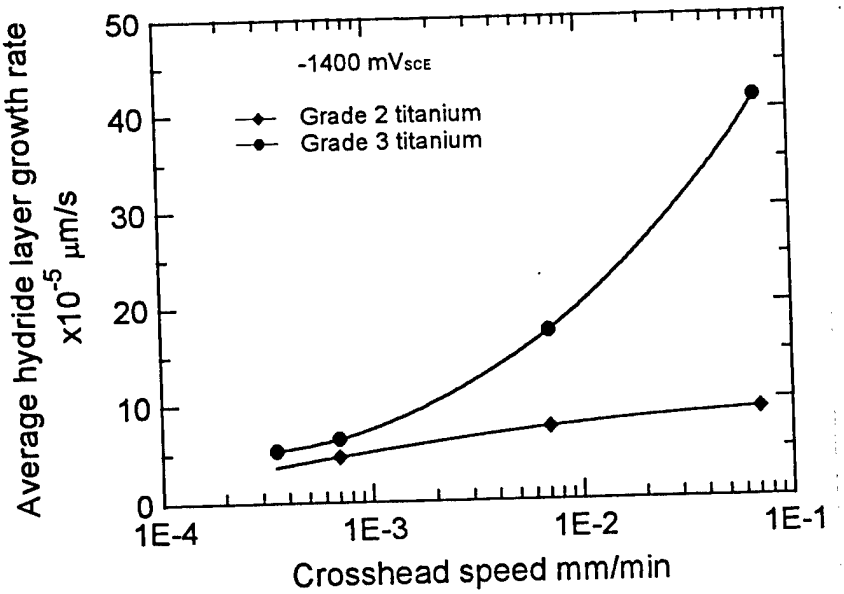

Figure 45 - Effect of applied crosshead speed on the average hydride layer growth rate on grade 2 and grade 3 titanium surfaces at -1400 mV_{SCE} at 70°C.

Figure 46 - Hydride layer covered on the fracture surface for grade 3 sample.

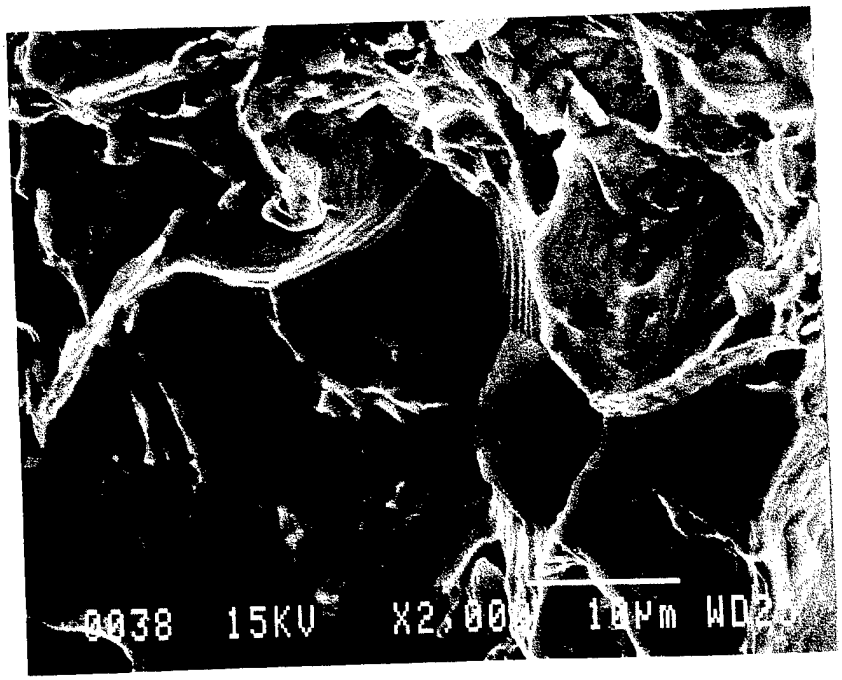

Figure 47 - Typical appearance of the fracture surface for grade 2 titanium at a potential of -700 mV_{SCE}, showing slip bands.

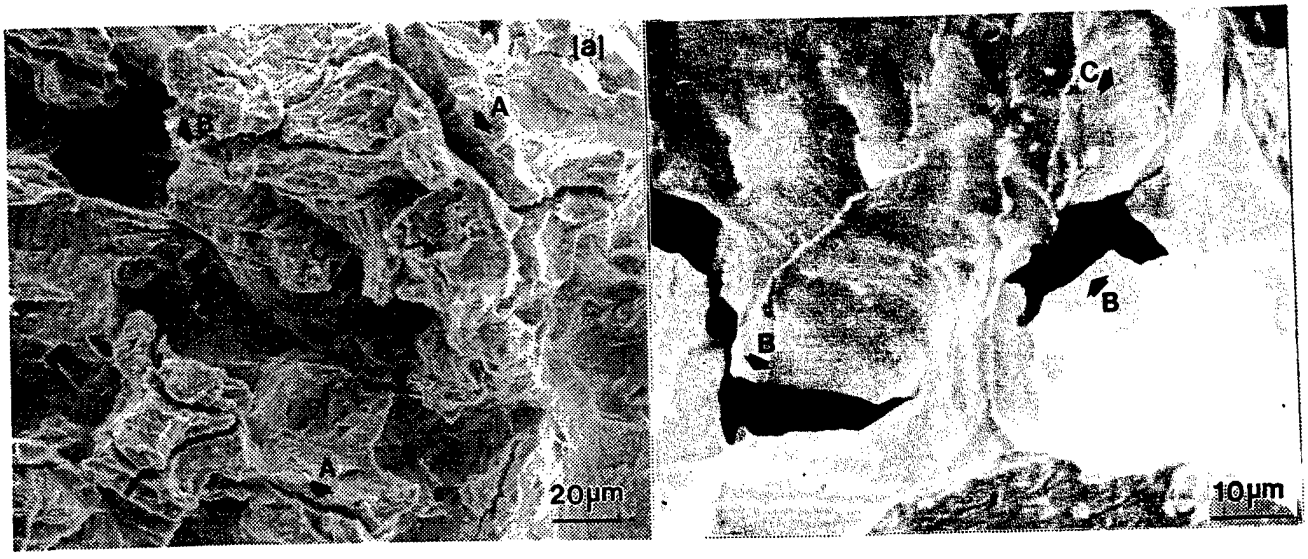

Figure 48 - Typical fracture surfaces of a sample of grade 2 titanium tested at -1200 mV_{SCE} (a) and grade 3 titanium tested at -1400 mV_{SCE} (b), showing secondary cracking A, micro-voids B and slip bands C.

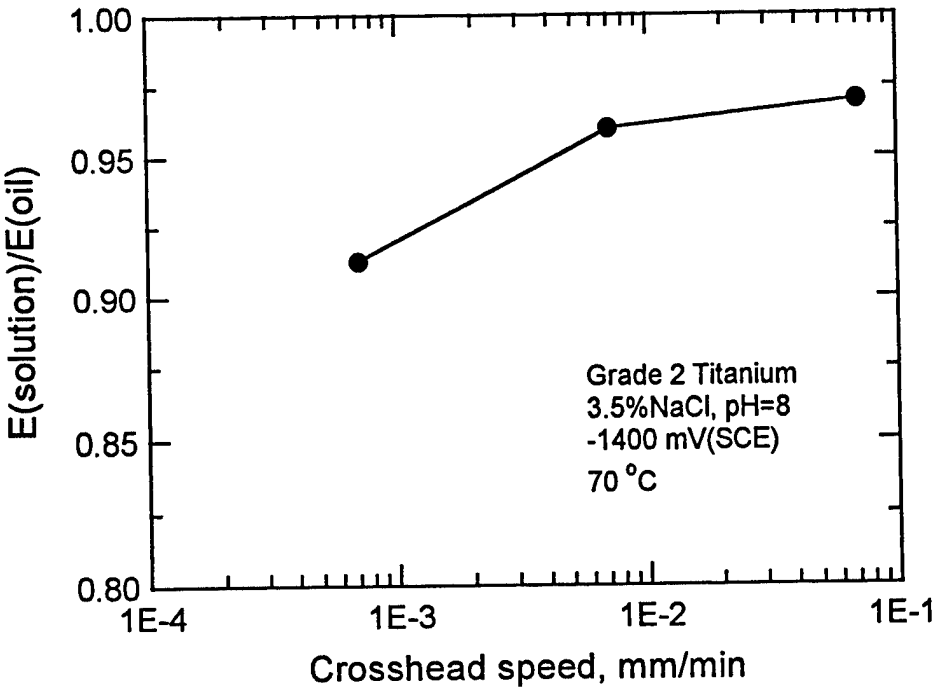

Figure 49 - The ratio of the elongation to failure in 3.5%NaCl (pH=8) to that obtained in oil plotted as a function of applied crosshead speed for grade 2 titanium at -1400 mV_{SCE} and 70°C.

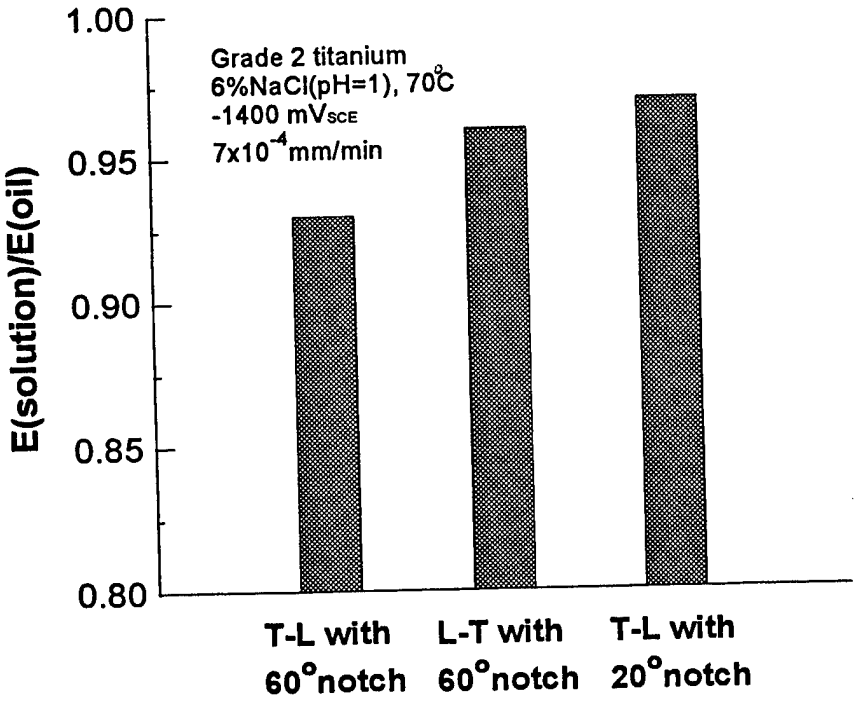

Figure 50 - The ratio of the elongation to failure in 6%NaCl (pH=1) to that obtained in oil for grade 2 titanium with different orientation and notch geometry tested at -1400 mV_{SCE} and 70°C.

Figure 51 - Cracks caused by hydride layer on grade 3 titanium sample, showing no hydride layer on the grade 3 titanium surface at the crack tip, (b) High mag of (a).

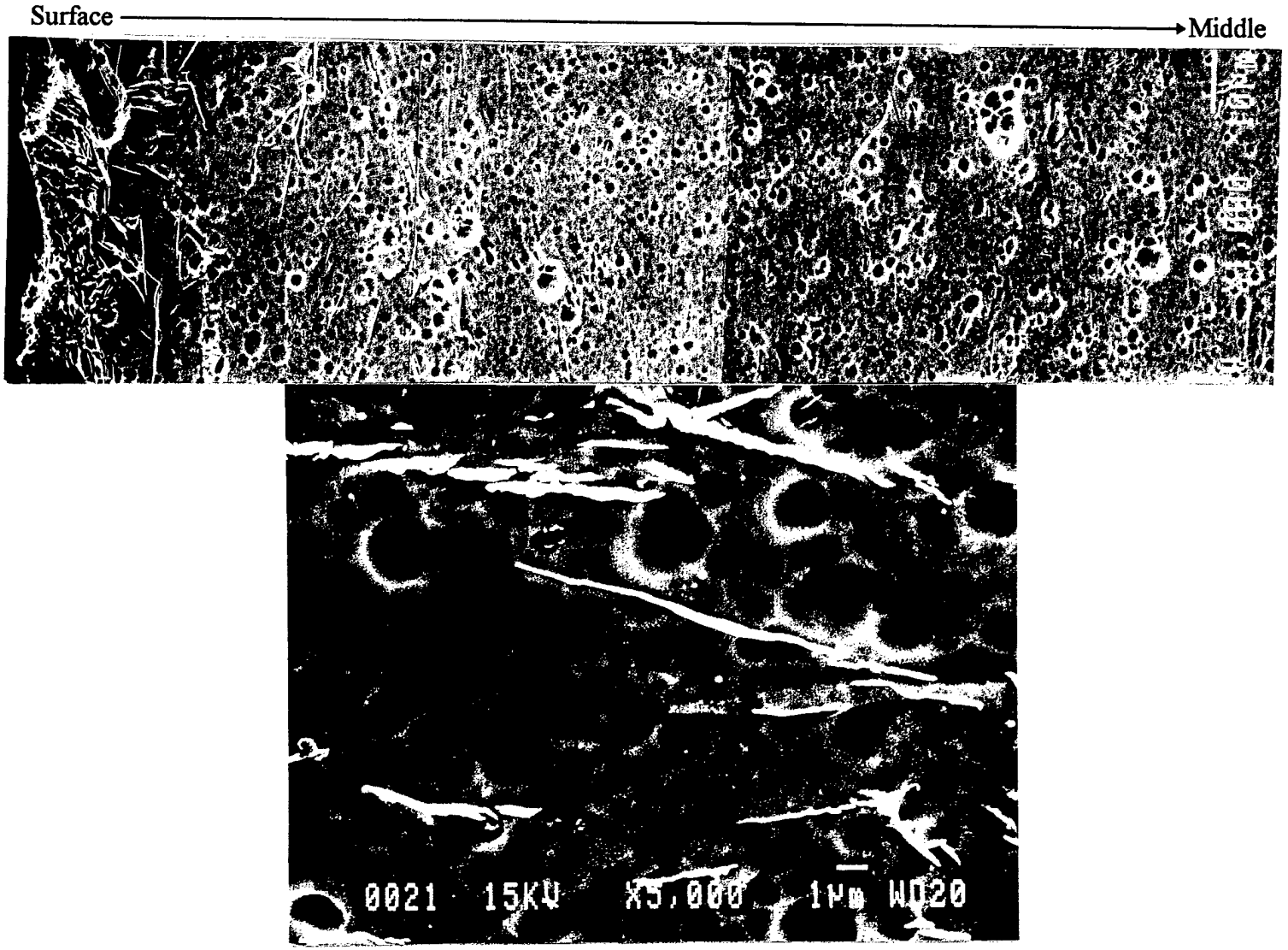

Figure 52 - Microstructure of grade 3 titanium after 5 days charging at -1400 mV_{SCE}, (a) near surface and (b) in the middle.

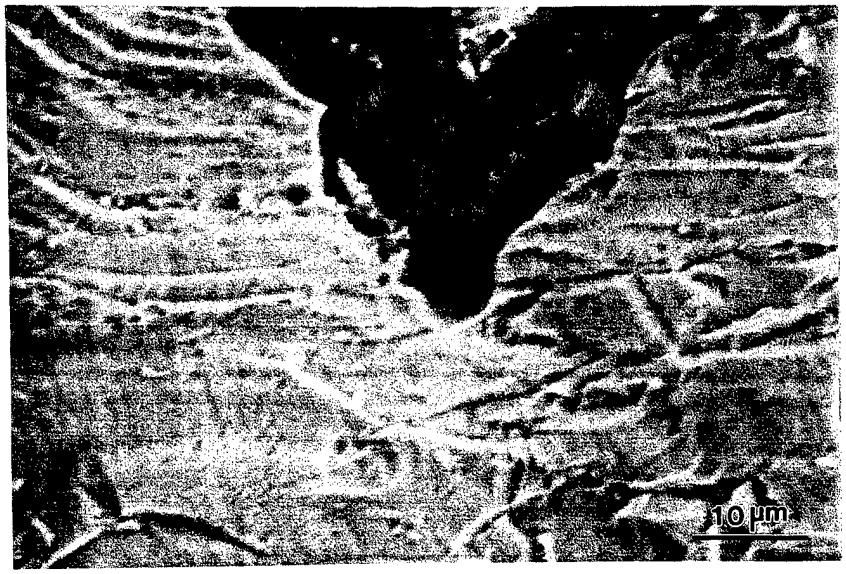

Figure 53 - The morphology of the crack tip for the grade 2 titanium sample after the test was terminated at point 1 in Fig. 4 in 6%NaCl solution at -1400 mV_{SCE} and 70°C.

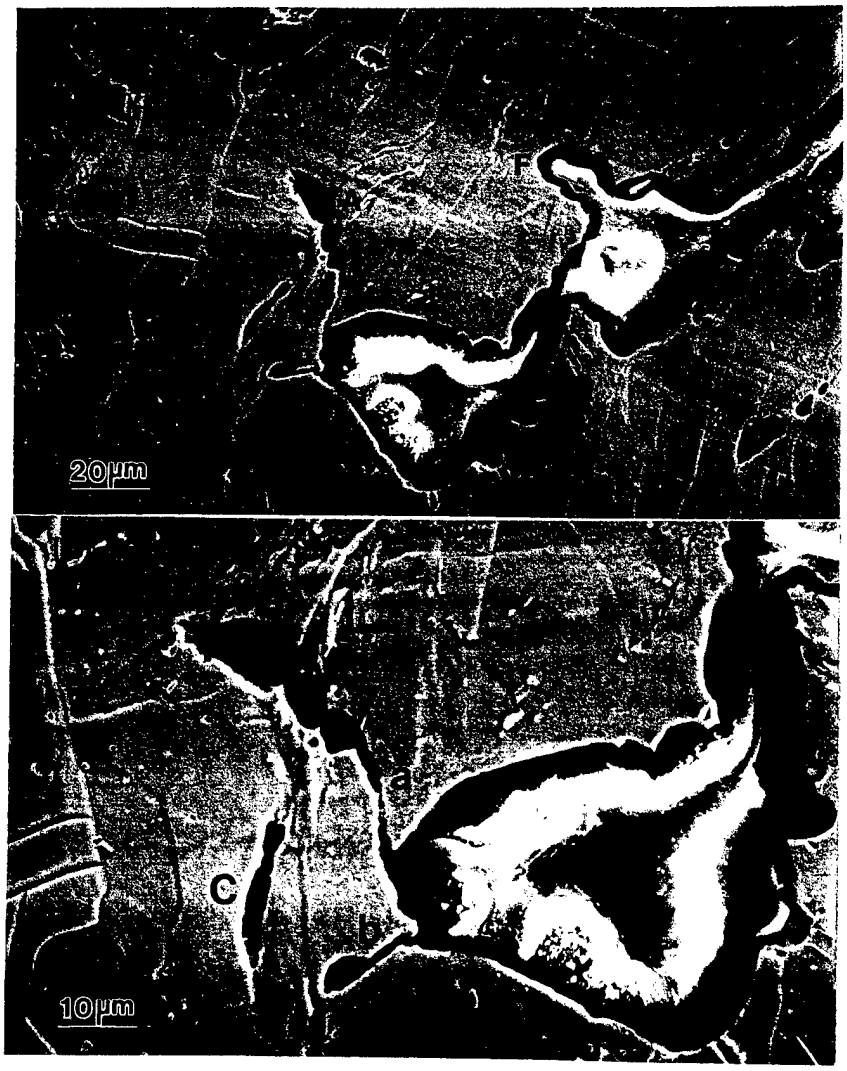

Figure 54 - The morphology of the crack tip for the grade 3 titanium sample after the test was terminated at point 1 in Fig. 4. The test was performed in 6%NaCl (pH=1) at -1400 mV_{SCE} and 70°C, (a) 500X and (b) 1000X.

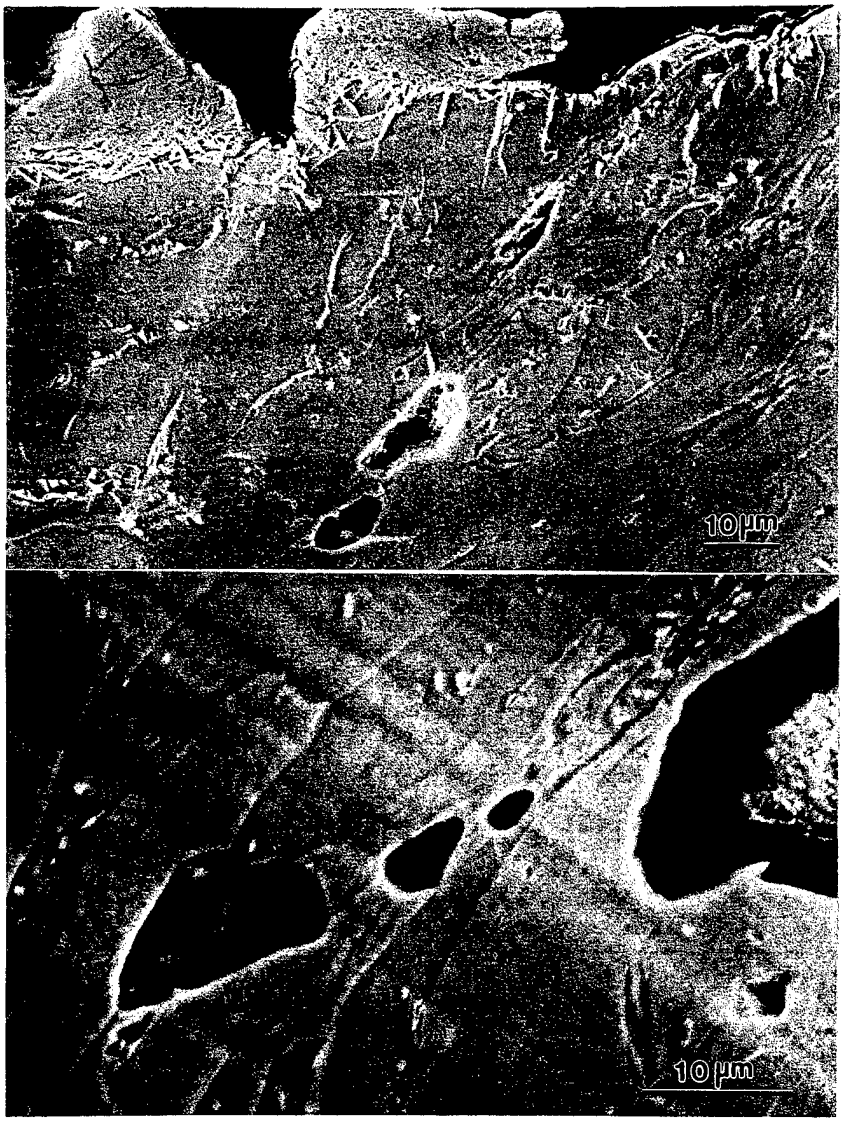

Figure 55 - Microcracks not oriented in the main crack path and therefore cannot connect to the main crack.

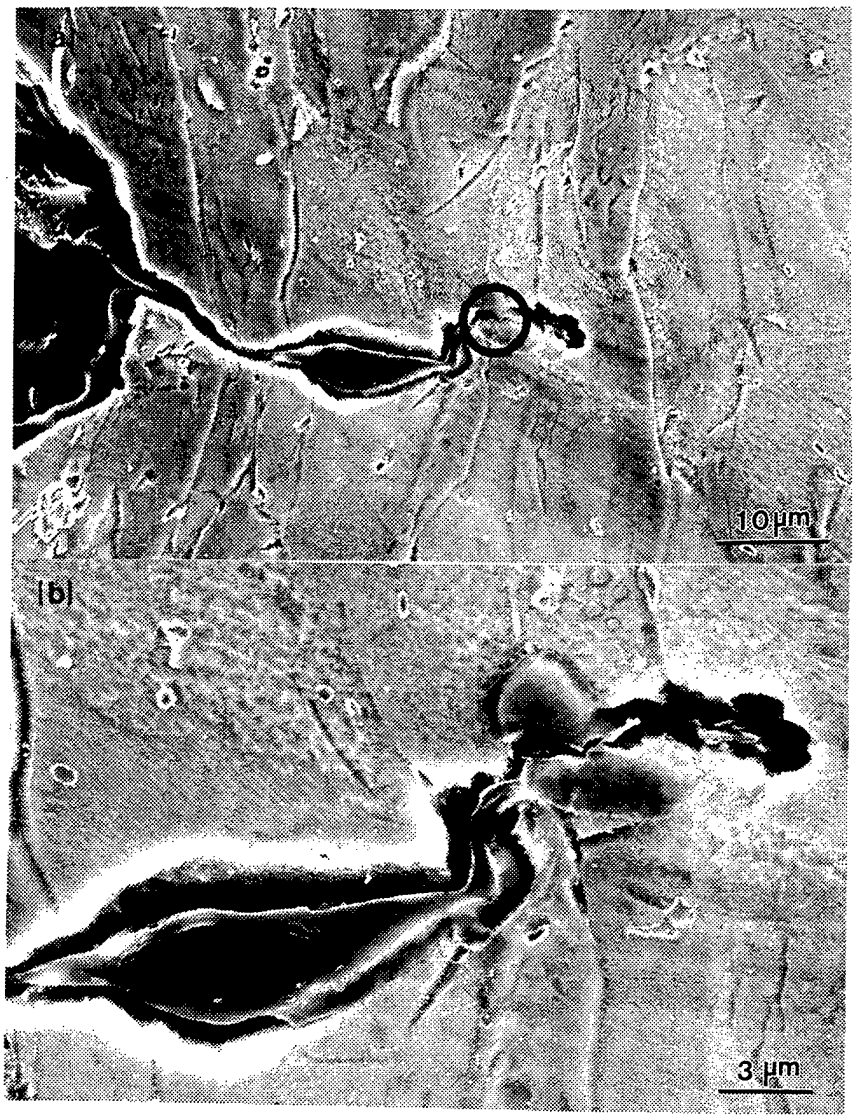

Figure 56 - The morphology of the crack tip for grade 3 titanium sample after test was terminated at point 2 in Fig. 4 tested at -1400 mV_{SCE} and 70°C, (a) 1500X and (b) 4000X.

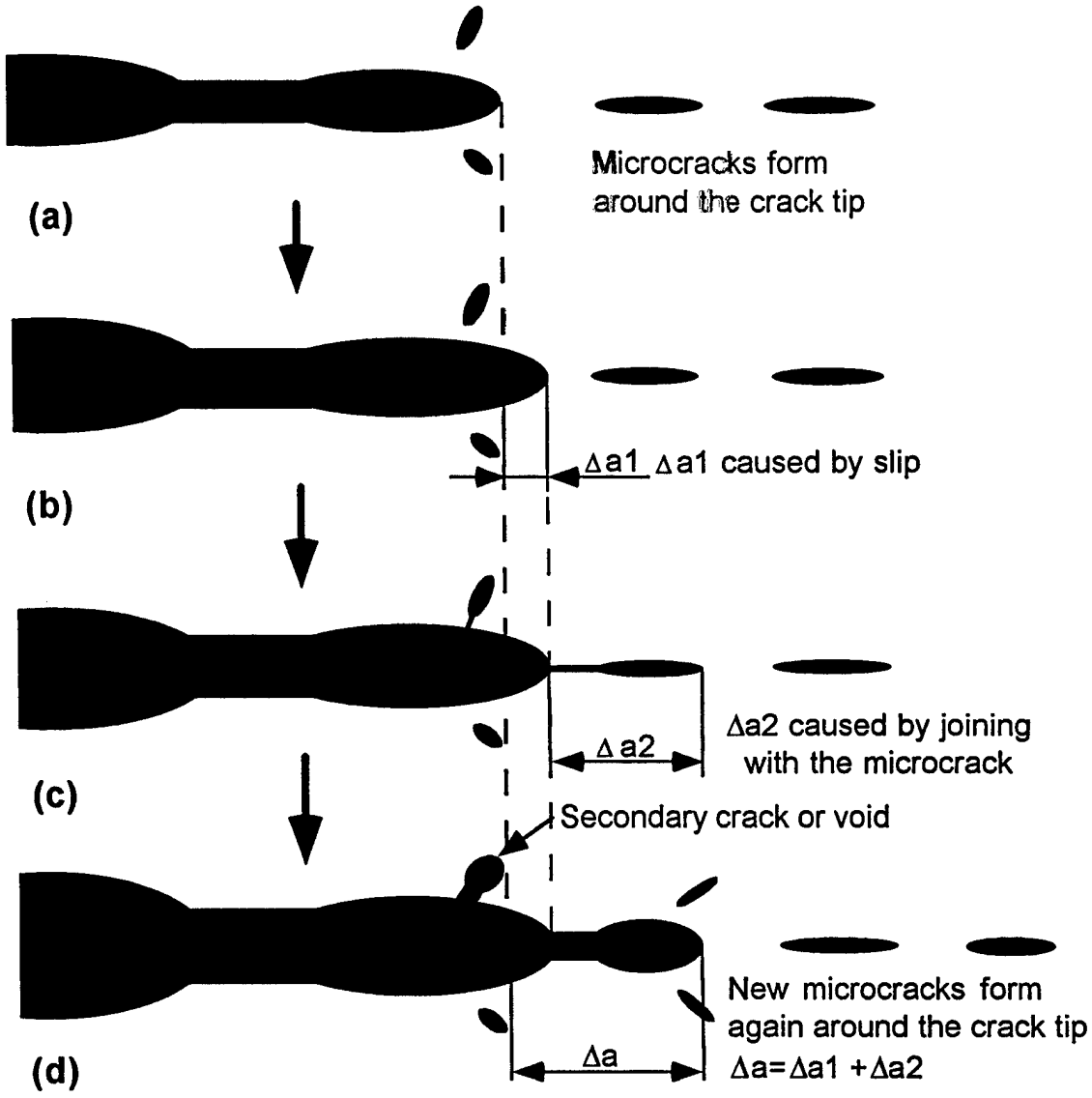

Figure 57 - Schematic diagram of the crack propagation mechanism. (a) microcracks formed around the crack tip caused by increased volume of hydride phases. (b) crack propagation caused by plastic slip. (c) crack propagation caused by joining with the microcrack. (d) new microcracks.

REPORT DOCUMENTATION PAGE

Form Approved
OMB No. 0704-0188

1. AGENCY USE ONLY (Leave blank)	2. REPORT DATE	3. REPORT TYPE AND DATES COVERED
	March 1998	Second Annual Report (1997)

4. TITLE AND SUBTITLE

Hydriding of Titanium

5. FUNDING NUMBERS

Grant No.
N00014-96-1-0272

6. AUTHOR(S)

Clyde L Briant, K. Sharvan Kumar, Zhengfu Wang

7. PERFORMING ORGANIZATION NAME(S) AND ADDRESS(ES)

Division of Engineering
Brown University
Box D, 182 Hope Street
Providence, RI 02912-9104

8. PERFORMING ORGANIZATION REPORT NUMBER

None

9. SPONSORING/MONITORING AGENCY NAME(S) AND ADDRESS(ES)

Office of Naval Research
800 N. Quincy Street
Arlington, VA 22217-5660

10. SPONSORING/MONITORING AGENCY REPORT NUMBER

11. SUPPLEMENTARY NOTES

None

12a. DISTRIBUTION/AVAILABILITY STATEMENT

Approved for public release; any or all parts of this document may be reproduced for use by U.S. Government

12b. DISTRIBUTION CODE

13. ABSTRACT *(Maximum 200 words)*

This report presents a summary of the second year of work on ONR Contract N00014-96-1-0272, Hydriding of Titanium. The reason for undertaking this work is that the US Navy would like to use titanium in a number of critical applications, where it would come in contact with sea water at elevated temperatures. Although the general reputation of titanium is that it is corrosion resistant in these environments, there is the possibility that it could pick up sufficient hydrogen from this environment to form a hydride and thus lose its mechanical integrity. Therefore, we must evaluate all conditions that could lead to hydriding and determine the effects of hydrides on mechanical properties. During the second year of work, the goals have been the following: to determine the effect of solution activity and temperature, material composition and heat treatment on the electrochemical properties of titanium; to determine the effect of these same variables on the corrosion potential of titanium galvanically coupled with other metals; to determine the critical potential of hydride formation as a function of solution activity and temperature, applied strain, and surface conditions; to measure the rate of hydrogen diffusion in titanium; to propose a model to describe crack propagation in titanium in these environments. All of the above work has been completed and the results are contained in this document.

14. SUBJECT TERMS	15. NUMBER OF PAGES
Titanium, hydrides, corrosion, galvanic corrosion, sea water, hydrogen embrittlement	63
	16. PRICE CODE

17. SECURITY CLASSIFICATION OF REPORT	18. SECURITY CLASSIFICATION OF THIS PAGE	19. SECURITY CLASSIFICATION OF ABSTRACT	20. LIMITATION OF ABSTRACT
unclassified	unclassified	unclassified	unlimited